Adaptation of *Bacillus subtilis* carbon core metabolism to simultaneous nutrient limitation and osmotic challenge: a multi-omics perspective

Michael Kohlstedt,[1,2] Praveen K. Sappa,[3]
Hanna Meyer,[4] Sandra Maaß,[5] Adrienne Zaprasis,[6]
Tamara Hoffmann,[6] Judith Becker,[1,2] Leif Steil,[3]
Michael Hecker,[5] Jan Maarten van Dijl,[7]
Michael Lalk,[4] Ulrike Mäder,[3] Jörg Stülke,[8]
Erhard Bremer,[6] Uwe Völker[3] and
Christoph Wittmann[1,2]*

[1]*Institute of Systems Biotechnology, Saarland University, Campus A1 5, 66123, Saarbrücken,*
[2]*Institute of Biochemical Engineering, Braunschweig University of Technology, Braunschweig,*
[3]*Interfaculty Institute of Genetics and Functional Genomics, Department Functional Genomics, University Medicine Greifswald,* [4]*Institutes of Biochemistry and* [5]*Microbiology, Ernst-Moritz-Arndt-University Greifswald, Greifswald,* [6]*Department of Biology, Laboratory of Microbiology, Philipps-University Marburg, Marburg, and* [8]*Department for General Microbiology, Georg-August-University Göttingen, Göttingen, Germany; and* [7]*Department of Medical Microbiology, University of Groningen, University Medical Center Groningen, Groningen, The Netherlands.*

Summary

The Gram-positive bacterium *Bacillus subtilis* encounters nutrient limitations and osmotic stress in its natural soil ecosystem. To ensure survival and sustain growth, highly integrated adaptive responses are required. Here, we investigated the system-wide response of *B. subtilis* to different, simultaneously imposed stresses. To address the anticipated complexity of the cellular response networks, we combined chemostat experiments under conditions of carbon limitation, salt stress and osmoprotection with multi-omics analyses of the transcriptome, proteome, metabolome and fluxome. Surprisingly, the flux through central carbon and energy metabolism is very robust under all conditions studied. The key to achieve this robustness is the adjustment of the biocatalytic machinery to compensate for solvent-induced impairment of enzymatic activities during osmotic stress. Specifically, increased production of several enzymes of central carbon metabolism compensates for their reduced activity in the presence of high salt. A major response of the cell during osmotic stress is the production of the compatible solute proline. This is achieved through the concerted adjustment of multiple reactions around the 2-oxoglutarate node, which drives metabolism towards the proline precursor glutamate. The fine-tuning of the transcriptional and metabolic networks involves functional modules that overarch the individual pathways.

Introduction

Frequently fluctuating environmental conditions force microbial cells to be highly adaptive and to remain in a vigilant state to cope with upcoming challenges (Hecker *et al.*, 2007). Cellular stress responses are complex and comprise extensive interconnected transcriptomic, enzymatic and metabolic adjustments to ensure survival and sustain growth under otherwise adverse conditions (Buescher *et al.*, 2012; Nicolas *et al.*, 2012). An increase in the external salinity is an important abiotic factor that affects the well-being and survival of microorganisms both in natural ecosystems and in industrial settings since it triggers a rapid and strong efflux of water from the cell (Record *et al.*, 1998) and thereby restricts, or even prevents, cell growth (Bremer and Krämer, 2000).

Bacillus subtilis is an endospore-forming bacterium that has long served as a model organism for Gram-positive microorganisms to study gene regulation, physiology and cellular differentiation processes (Sonenshein *et al.*, 2003; Lopez *et al.*, 2009). It lives in a challenging habitat, the upper layers of the soil (Earl *et al.*, 2008), where nutrient limitations impair growth and where desiccation processes create sustained high-salinity and high-osmolarity micro-niches (Bremer, 2003). *B. subtilis* is not only a model organisms widely used to study basic

biological processes (Sonenshein *et al.*, 2003); it is also a biotechnologically important industrial workhorse for producing technical enzymes, vitamins, antibiotics, and specialty chemicals (Harwood, 1992; Schallmey *et al.*, 2004; van Dijl and Hecker, 2013). During high-cell density fermentation processes, the producer cells will experience a strong hyperosmotic burden caused by substrate feed and the increase in product titres (Schweder *et al.*, 1999) thereby limiting the overall productivity of the *B. subtilis* cell factory.

High-salinity-triggered osmotic up-shocks are among the best inducers of the SigB-controlled general stress response regulon of *B. subtilis* (Hecker *et al.*, 2007). This complex system provides the cell with both acute and pre-emptive resistance against a multitude of environmental and cellular challenges and nutritional constraints (Hecker *et al.*, 2007; Price, 2011). Indeed, many members of the general stress response system contribute to cellular survival upon a severe osmotic up-shift (Höper *et al.*, 2005; 2006). However, due to the transient nature of the induction of the SigB regulon after a salt shock (Spiegelhalter and Bremer, 1998; Hahne *et al.*, 2010; Nannapaneni *et al.*, 2012; Young *et al.*, 2013), it cannot provide adequate protection for cells cultured under sustained high-salinity conditions (Spiegelhalter and Bremer, 1998). Under these circumstances, the cell initially imports large quantities of potassium ions as an emergency stress reaction to restrict water loss (Whatmore and Reed, 1990; Holtmann *et al.*, 2003). In the ensuing adaptation phase to persistent high salinity, *B. subtilis* reduces the size of the potassium pool again, and hence the ionic strength of the cytoplasm, by partially replacing it with compatible solutes (Whatmore *et al.*, 1990). These organic osmolytes are highly congruous with cellular biochemistry and physiology (Kempf and Bremer, 1998; Fisher, 2006; Street *et al.*, 2006), features that allow their cellular accumulation to exceedingly high intracellular concentrations. Hence, water retention and maintenance of vital turgor by high osmolarity-challenged cells is ensured. Glycine betaine and L-proline are two important representatives of the compatible solutes (Kempf and Bremer, 1998).

The only compatible solute that *B. subtilis* can synthesize *de novo* is L-proline (Whatmore *et al.*, 1990; Brill *et al.*, 2011a), and its cellular pool increases from about 10–20 mM in cells grown in chemically defined standard laboratory media to about 500 mM in cells experiencing a severe continued salt stress (e.g. media containing 1.2 M NaCl) (Hoffmann *et al.*, 2013; Zaprasis *et al.*, 2013). Genetic disruption of the osmostress-adaptive proline biosynthetic pathway causes osmotic sensitivity (Brill *et al.*, 2011a). *B. subtilis* can also protect itself against the detrimental effects of these growth conditions by importing preformed compatible solutes (e.g.

glycine betaine) (Boch *et al.*, 1994; Nau-Wagner *et al.*, 2012).

Effective water management is certainly at the core of the *B. subtilis* cell's response to salt and osmotic stress (Bremer and Krämer, 2000; Bremer, 2003), but the cellular acclimatization to persisting high osmolarity is a multifaceted and well-staged process (Steil *et al.*, 2003; Höper *et al.*, 2006; Hahne *et al.*, 2010; Nicolas *et al.*, 2012). Many questions remain and a more comprehensive understanding of cellular activities under salt stress growth conditions would be highly relevant for both basic research and industrial applications. One of the key questions that arise from the current knowledge revolves around the massive *de novo* synthesis of proline in osmotically stressed cells and the adaptation(s) of the central metabolism to produce this compatible solute. This issue is even more critical if one considers that salt stress and nutrient limitation usually occur simultaneously in soil, the natural habitat of *B. subtilis*.

Here, we have taken a systems biology perspective (Kohlstedt *et al.*, 2010) to address these questions with a particular focus on the cellular events that shape the central carbon metabolism of *B. subtilis* under continued salt stress. To this end, we applied transcriptomic, mass spectrometry-based proteomic, metabolomic and ^{13}C-fluxomic techniques to cells grown under well-controlled conditions in a glucose-limited chemostat. We integrated the derived rich datasets into a carefully curated picture of the physiological adaptations that permit *B. subtilis* to grow in a sustained high-salinity environment that is simultaneously limited for carbon supply.

Results

Physiological adaptation to carbon-limited growth under salt stress and osmoprotection by glycine betaine

The system-wide response of *B. subtilis* cells to salt stress and the effects of the potent osmoprotectant glycine betaine (Boch *et al.*, 1994) were assessed in chemostat cultures at a dilution rate of 0.1 h^{-1}. These conditions were chosen from screening experiments at different salt levels (see Supporting Information Fig. S1). The identical growth rate imposed in all experiments allowed to exclude potential growth effects that could have emerged from different growth rate management (Goelzer and Fromion, 2011). The experiments comprised an unperturbed reference, a high-salinity environment (1.2 M NaCl) and a set-up where the high-salinity-challenged cells were protected with the compatible solute glycine betaine (1.2 M NaCl, 1 mM glycine betaine). Salt stress somewhat decreased the biomass yield, which, however, was partially restored by the addition of glycine betaine (Table 1). In the presence of high salt, cells produced slightly more CO_2 and secreted trace

Table 1. Physiological data and carbon balance for *Bacillus subtilis* BSB1 (168 Trp[+]) during chemostat growth in M9 minimal medium without further addition (reference), supplemented with 1.2 M NaCl (salt stress), and supplemented with 1.2 M NaCl and 1 mM glycine betaine (osmoprotection).

|	Unit	Reference	Salt stress	Osmoprotection
$Y_{X/S}$	g_{DCW} mol^{-1}	55.6 ± 5.8	44.1 ± 2.4	48.7 ± 3.2
q_S	mmol g_{DCW}^{-1} h^{-1}	1.8 ± 0.2	2.3 ± 0.1	2.1 ± 0.1
q_{CO2}	mmol g_{DCW}^{-1} h^{-1}	6.7 ± 0.2	7.3 ± 0.3	7.6 ± 0.1
$q_{acetate}$	µmol g_{DCW}^{-1} h^{-1}	10.9 ± 1.1	12.0 ± 1.8	15.5 ± 3.3
$q_{pyruvate}$	µmol g_{DCW}^{-1} h^{-1}	1.3 ± 0.3	3.7 ± 0.3	1.5 ± 0.5
$q_{succinate}$	µmol g_{DCW}^{-1} h^{-1}	0.6 ± 0.2	1.1 ± 0.3	< 0.1
$q_{lactate}$	µmol g_{DCW}^{-1} h^{-1}	6.8 ± 1.4	< 0.1	< 0.1
$q_{oxoglutarate}$	µmol g_{DCW}^{-1} h^{-1}	< 0.1	$6.7 + 1.1$	7.0 ± 2.0
$q_{isobutyrate}$	µmol g_{DCW}^{-1} h^{-1}	3.0 ± 1.2	29.2 ± 4.8	10.4 ± 2.6
$q_{isobutyrate}$	µmol g_{DCW}^{-1} h^{-1}	3.4 ± 1.5	11.0 ± 2.0	9.4 ± 1.8
q_{valine}	µmol g_{DCW}^{-1} h^{-1}	< 0.1	36.7 ± 6.9	< 0.1
$q_{leucine}$	µmol g_{DCW}^{-1} h^{-1}	< 0.1	21.6 ± 2.8	< 0.1
$q_{protein}$	mg g_{DCW}^{-1} h^{-1}	26.6 ± 3.6	47.9 ± 2.6	53.2 ± 1.8
C recovery[a]	%	98.3 ± 6.5	98.6 ± 6.8	101.4 ± 4.6

The data comprise biomass yield ($Y_{X/S}$), specific rates for glucose uptake (q_S) and extracellular product formation ($n = 4$).
a. The estimation of the carbon balance considered the measured carbon content of the biomass, which was 44.3 ± 0.1 (reference), 44.2 ± 1.0 (salt-stress) and $42.9 \pm 0.9\%$ (osmoprotection). To account for the extracellular protein, a relative fraction of 53.5% carbon was deduced from the protein composition of *B. subtilis* (Sauer *et al.*, 1996). The residual glucose level in the medium did not differ between the conditions (25 ± 9 µM).

amounts of leucine and valine. However, extracellular metabolite formation was generally weak under all conditions. The recorded physiological data matched perfectly with the calculated carbon balance for all conditions, as indicated by the complete recovery of the assimilated substrate carbon in cell biomass, CO_2, extracellular metabolites and secreted protein (Table 1).

The chemostat cultures were also sampled for multiomics analysis. Prior to a more detailed investigation, the omics datasets were first evaluated statistically, using principal component analysis (Fig. 1). The individual replicates f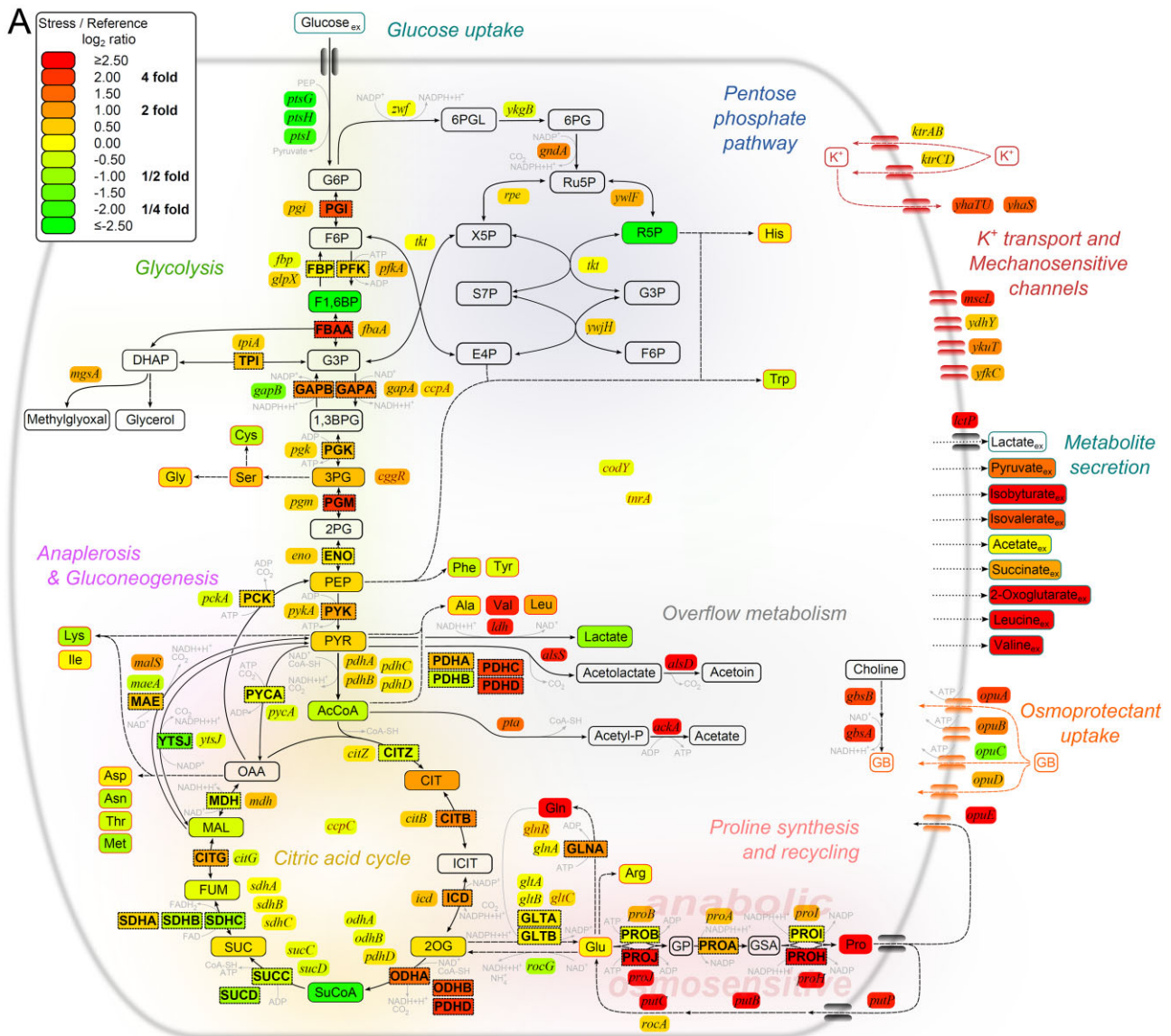or each growth condition showed high similarity at the transcriptome, proteome and metabolome levels, as indicated by their tight clustering within 95% confidence ellipses. At the same time, cells from all three scenarios of cell growth differed remarkably from each other on the level of the cellular components highlighting the different physiological states of the cultures. It is interesting to note in this context that the cellular state of the salt-challenged cells attained through osmoprotection by glycine betaine did not resemble that of the reference culture grown in the absence of additional salt. Instead, it represented a new, clearly different metabolic mode of *B. subtilis*.
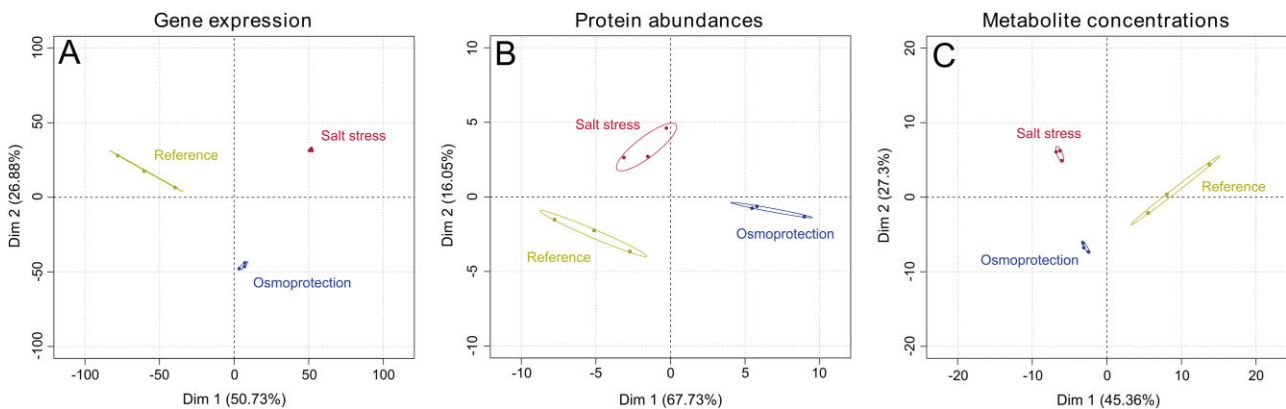
Fig. 1. Principal component analysis plots of generated datasets.
A. Gene expression data from 4105 genes obtained by microarray analysis.
B. Protein abundance of 39 central carbon metabolism enzymes comprising Embden-Meyerhof-Parnas pathway, citric acid cycle, gluconeogenesis, glutamine, glutamate and proline synthesis.
C. Concentrations of 109 intra- and extracellular metabolites. Each replicate of a condition is represented by one data point. Clustering replicates are surrounded by 95% confidence ellipses.

Fig. 2. Integrated view of relative transcript, protein and metabolite concentrations.
A. Data from salt-stressed cells (in the presence of 1.2 M NaCl) is compared with control conditions without additional salt.
B. Data from protected salt-stressed cells (in the presence of 1.2 M NaCl and 1 mM glycine betaine) is compared with salt-stressed cells (without GB).
The data format is as follows: gene expression, *italics*; protein abundance, dashed rectangle; metabolite pool, round-shaped solid rectangle.

Stress response during carbon-limited growth is modulated by compatible solutes

The only compatible solute that *B. subtilis* can synthesize *de novo* is proline (Whatmore *et al.*, 1990; Brill *et al.*, 2011a). *B. subtilis* possesses two pathways for the synthesis of proline from glutamate: (i) The anabolic route is catalysed by the ProB-ProA-ProI enzymes whose genetic and biochemical regulation indicates that this pathway is essential for protein biosynthesis. This pathway produces cellular proline pools between 10–20 mM

(Whatmore *et al.*, 1990; Brill *et al.*, 2011b; Hoffmann *et al.*, 2013). (ii) The osmostress-adaptive route involves the ProJ-ProA-ProH enzymes. This pathway allows to attain cellular proline pools up to 0.5 M in response to the severity of the imposed osmotic stress (Whatmore *et al.*, 1990; Brill *et al.*, 2011a; Hoffmann *et al.*, 2013; Zaprasis *et al.*, 2013). In our multi-omics analysis, the increased formation of proline at high osmolarity was reflected by the accumulation of mRNAs and proteins of the osmostress-responsive route (Fig. 2A). In particular, the amount of the *proH-proJ* mRNA was increased about sevenfold
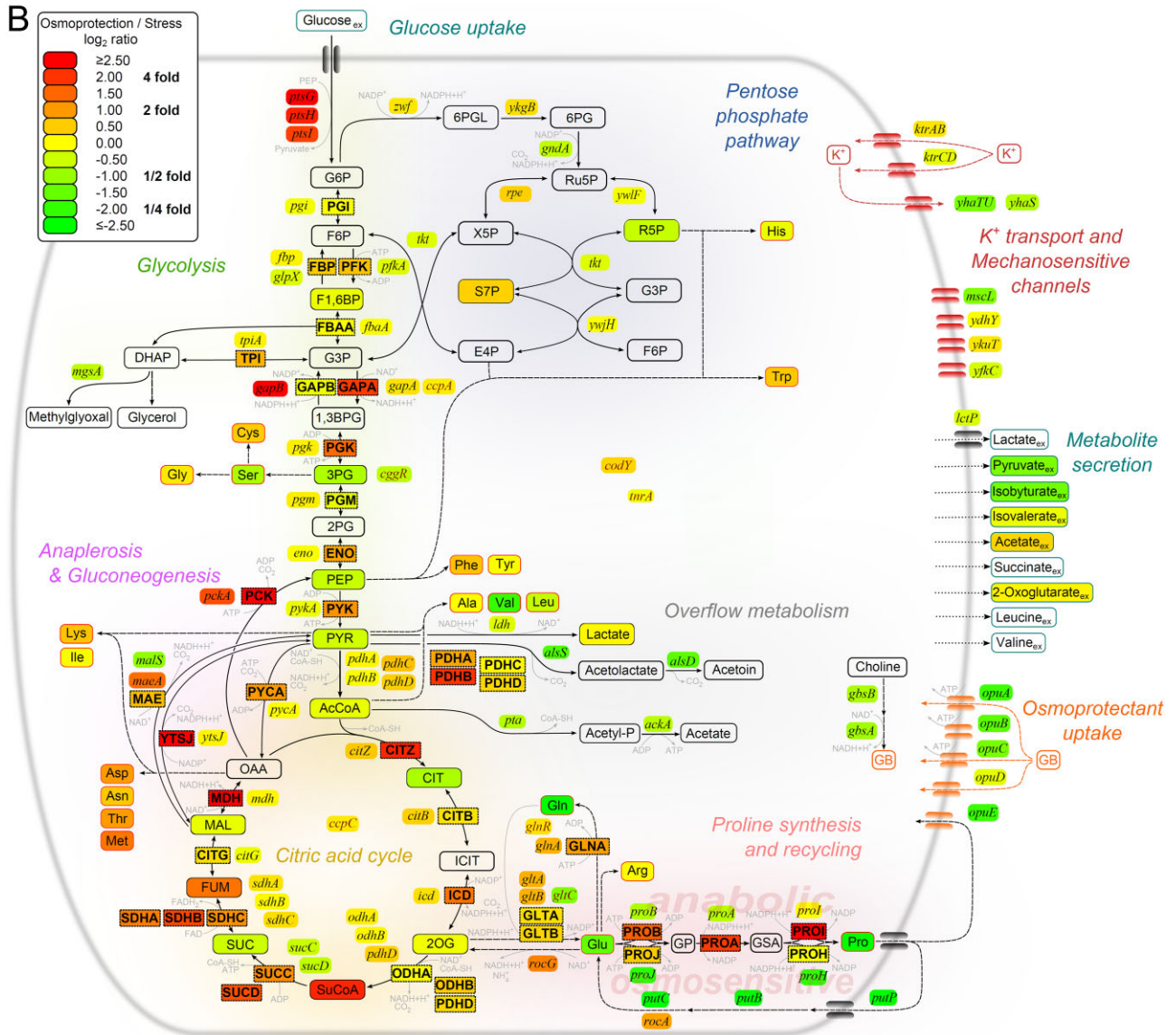
Fig. 2. *cont.*

under osmotic stress conditions, and a corresponding upregulation in the amounts of the ProH and ProJ enzymes was observed. In contrast, the cellular level of the ProA protein remained almost unchanged, a finding that is fully in agreement with the observation that *proA* transcription is not osmotically inducible (Brill *et al.*, 2011a). Interestingly, the *putBCP* operon encoding the proline transporter PutP and the two catabolic enzymes PutB and PutC (Moses *et al.*, 2012) were among the most strongly induced operons under high-salinity growth conditions. The mRNA of the promoter-distal *putP* gene accumulated about 20-fold during growth

in the presence of 1.2 M NaCl. The expression of the glutamate synthase complex (GltAB) slightly decreased in presence of high salt, despite increased requirement to produce the proline precursor glutamate (Gunka and Commichau, 2012). In the presence of externally added glycine betaine, expression of the osmostress-responsive proline biosynthesis pathway was significantly reduced (Fig. 2B), but still occurred above the level observed in control cells. This observation is in excellent agreement with the recently reported finely tuned repressing effect of glycine betaine on the cellular proline pool (Hoffmann *et al.*, 2013).

Flux measurements indicate robustness of the carbon core metabolic network and precise regulation to meet the demand for proline at high salinity

The impact of salt stress and osmoprotection by glycine betaine was explored in more detail on the level of carbon fluxes. Under reference conditions, *B. subtilis* exhibited parallel operation of the pentose phosphate pathway (PPP) and the Embden-Meyerhof-Parnas pathway (Fig. 3A). At the PEP-pyruvate-oxaloacetate node, fluxes through PEP carboxykinase, pyruvate kinase and pyruvate carboxylase or through the so-called pyruvate shunt via the malic enzyme allowed anaplerotic fuelling of the TCA cycle. This contributes to the supply of energy and reducing power (NADPH) for biosynthetic reactions. The observed fluxes agreed well with recent estimates under similar growth conditions (Tännler *et al.*, 2008). Figure 3B highlights the flux response of *B. subtilis* to salt stress. Remarkably, osmotically stressed cells maintained a robust substrate flux through the core metabolic network. Distinct changes of the flux distribution were only observed at the 2-oxoglutarate node. Here, flux was redirected from the TCA cycle towards glutamate, and then to glutamine and proline. The glutamate pool remained constant at about 700 µmol g_{DCW}^{-1}. The intracellular glutamine and proline pools in control cells occurred at levels of 30 and 60 µmol g_{DCW}^{-1}, respectively, and their concentrations increased 15- and 20-fold, respectively, under salt stress conditions. The elevated NADPH demand for biosynthesis of these amino acids apparently triggered the flux increase into the PPP that delivers this critical cofactor. Furthermore, fluxes at the pyruvate node partly switched from TCA cycle anaplerosis to increased intracellular levels of the branched chain amino acids valine and leucine and branched chain keto acids derived from them (Fig. 2B). These flux changes at the 2-oxoglutarate and pyruvate nodes were not observed when glycine betaine was added to salt-stressed cells. Thus, the flux towards glutamate-based amino acids and pyruvate-based metabolites (Fig. 3C) and consequently the intra- and extracellular levels of these compounds and their precursors were reduced in comparison with salt-stressed cells (Fig. 2B). Importantly, the PPP flux also decreased under conditions of osmoprotection by glycine betaine, an observation that is in excellent agreement with the reduced demand for *de novo* synthesis of the osmostress protectant proline. Interestingly, the remaining flux backbone was robustly maintained.

A fundamental determinant of cellular physiology is the energetic state, which can be quantified by the ratio between energy rich and energy poor adenylate nucleotides, referred to as the adenylate energy charge (AEC) (Atkinson, 1968). By upholding flux homeostasis through large parts of the metabolic network, the cells maintained their high-energy status under salt stress and under osmostress protection conditions, as compared with reference cells (Table 2).

B. subtilis *displays distinct transcriptional adaptations in its core metabolic pathways to counteract osmotic stress*

Hierarchical cluster analysis of expression patterns for genes of carbon core and proline metabolism revealed pronounced responses (Figs. 2A and 4). Salt stress stimulated the expression of genes physiologically connected with overflow pathways for the production of acetoin, acetate and lactate. These changes were reversed under conditions of cellular osmoprotection by glycine betaine. In agreement with the increased demand for proline in salt-challenged cells, salt stress moderately induced virtually all genes of Embden-Meyerhof-Parnas pathway and of the TCA cycle down to the 2-oxoglutarate node, whereas the downstream part of the TCA cycle was not activated. This observation is in full agreement with previous data derived from a comprehensive proteome analysis of severely salt-shocked cells (Höper *et al.*, 2006).

The gluconeogenic genes *pckA* (PEP carboxykinase) and *gapB* (glyceraldehyde-3-phosphate dehydrogenase) were slightly repressed at high salt. The inverse regulation of glycolytic and gluconeogenic genes is in good agreement with previous studies (Fillinger *et al.*, 2000). The genes *gndA* and *malS* encoding gluconate 6-phosphate dehydrogenase and a decarboxylating malic enzyme, respectively, were upregulated under salt stress. Both enzymes are involved in intracellular balancing of NADPH (Rühl *et al.*, 2012). Overall, gene expression changes indicated concerted activation of the full biosynthetic chain from glucose 6-phosphate, the entry point of the substrate glucose into cellular metabolism, to the osmoprotectant proline; hence, adjustments in metabolism across multiple pathways occur. It is interesting to note that the underlying change in gene expression comprised co-regulated modules (Fig. 4). These modules mainly contained genes from pyruvate-based overflow metabolism and osmostress-adaptive proline synthesis (cluster a), ammonium metabolism and TCA cycle (cluster b), glutamate and glutamine synthesis (cluster c) and Embden-Meyerhof-Parnas pathway (cluster d). Together, expression of these modules is adjusted in a way to (i) keep the core metabolic fluxes even under the simultaneously imposed nutrient limitation and salt stress, and (ii) provide the cell with the metabolic resources to synthesize the vast amounts of proline required to protect it against the detrimental effects of high salinity. It is apparent from our analysis that precise and co-ordinated adjustments in carbon
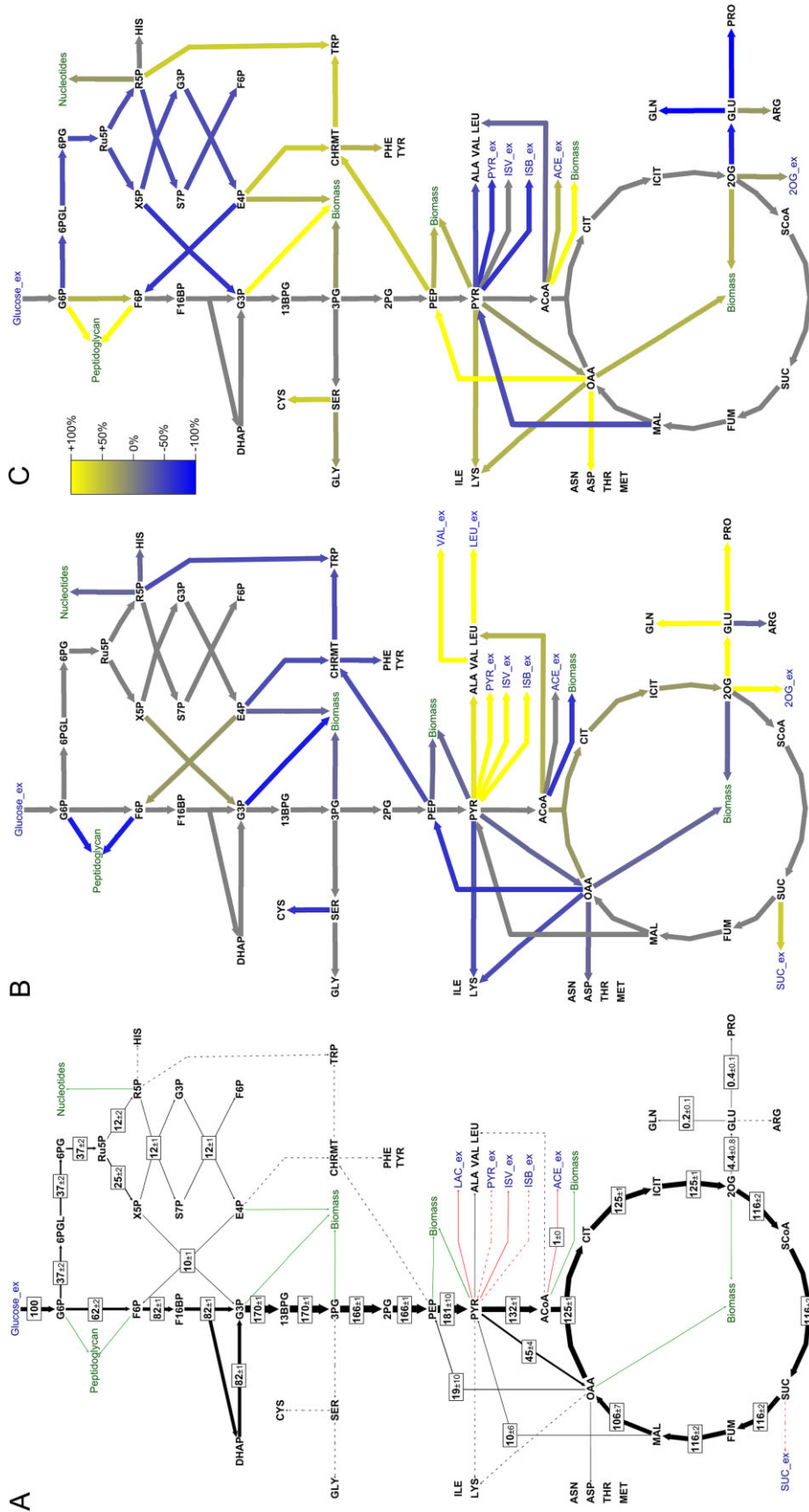
Fig. 3. Relative changes in metabolic flux distribution.
A. Relative carbon flux distribution under reference conditions normalized to the specific glucose uptake rate ($q_S = 1.82$ mmol g_{DCW}^{-1} h^{-1}). The errors given represent 90% confidence intervals of the estimated fluxes.
B. Flux change in percent in salt-stressed cells compared with non-stressed cells.
C. Flux change in percent in glycine betaine-protected cells compared with salt-stressed cells. Arrow colors indicate positive (yellow) and negative (blue) flux changes. Unchanged fluxes are given as gray arrows. Non-standard abbreviations for metabolites: ACE, acetate; ACoA, acetyl-coenzyme A; CHRMT, chorismate; CIT, citrate; DHAP, dihydroxyacetone phosphate; E4P, erythrose 4-phosphate; F6P, fructose 6-phosphate; F16BP, fructose 1,6-bisphosphate; FUM, fumarate; G6P, glucose 6-phosphate; G3P, glyceraldehyde 3-phosphate; 13BPG, 1,3-bisphosphoglycerate; 2PG, 2-phosphoglycerate; 3PG, 3-phosphoglycerate; ISB, isobutyrate; ICIT, isocitrate; ISV, isovalerate; LAC, lactate; MAL, malate; OAA, oxaloacetate; 2OG, 2-oxoglutarate; 6PG, 6-phosphogluconate; 6PGL, 6-phosphogluconolactone; PEP, phosphoenolpyruvate; PYR, pyruvate; R5P, ribose 5-phosphate; Ru5P, ribulose 5-phosphate; S7P, sedoheptulose 7-phosphate; SUC, succinate; SCoA, succinyl-coenzyme A; X5P, xylulose 5-phosphate The amino acids are abbreviated according to the standard three letter code.

Table 2. Intracellular levels of nucleotides for non-stressed, salt-stressed and osmoprotected *B. subtilis* cells, grown in chemostat cultures at 0.1 h^{-1} ($n = 3$).

	Unit	Reference	Salt stress	Osmoprotection
AMP	µmol g$_{DCW}^{-1}$	1.9 ± 0.5	1.5 ± 1.4	1.2 ± 0.5
ADP	µmol g$_{DCW}^{-1}$	4.1 ± 0.6	5.8 ± 3.3	2.8 ± 0.3
ATP	µmol g$_{DCW}^{-1}$	19.2 ± 2.3	17.4 ± 6.8	6.3 ± 1.4
GTP	µmol g$_{DCW}^{-1}$	5.2 ± 2.5	1.7 ± 0.4	1.4 ± 0.3
AEC	–	0.84 ± 0.03	0.83 ± 0.04	0.75 ± 0.02

The energy level is expressed by the adenylate energy charge (AEC) (Atkinson, 1968).

metabolism are required to achieve this complex physiological task.

Salt stress and osmoprotection of salt-stressed cells resulted in a variety of additional responses in gene expression beyond the central carbon metabolism. We do not consider these changes any further here, but we fully document them in the supplementary material (see Supporting Information Fig. S1, Appendix S1, GSE53333).

Glycine betaine restores the expression of carbon core metabolic genes

Glycine betaine is a very effective osmoprotectant for *B. subtilis* with pronounced beneficial effects on cell growth (Boch *et al.*, 1994). However, it is so far unclear whether osmotically stressed cells cultivated in the presence of this osmoprotectant fully revert to the physiological reference state of cells not challenged by osmotic stress. A prominent consequence of the accumulation of glycine betaine under osmotic stress conditions is a strong reduction of the proline pool generated by *de novo* synthesis (Hoffmann *et al.*, 2013). Indeed, osmotically stressed cells cultivated in the presence of glycine betaine substantially reduced the osmostress-adaptive proline biosynthetic route in our experiments as well (Fig. 2B). Furthermore, the expression of the genes constituting the carbon core metabolic network was restored to the levels observed under reference conditions (i.e. in the absence of salt stress). While the expression levels of most of these genes were fully restored, the reversion of the expression levels of few genes did not reach or exceed the reference levels (see Fig. 4). In particular, this was observed for the genes for overflow metabolism and the *pckA* and *gapB* gluconeogenic genes respectively.

It is interesting to note that despite the restoration of gene expression of carbon core metabolism in the presence of the osmoprotectant glycine betaine, the overall gene expression state of osmoprotected cells differed substantially from that of both reference and stressed cells (see Fig. 1). Interestingly, the restored gene expression of the carbon core metabolic network was not reflected by the proteomes and metabolomes (see Fig. 2).

This supports the idea that not all physiological changes in a cell can be traced back to alterations in gene expression (Schilling *et al.*, 2007; Chubukov *et al.*, 2013). To resolve this issue further, we next investigated the effects of salt stress and glycine betaine at the levels of protein accumulation and protein activity in more detail.

B. subtilis *responds to osmotic stress and osmoprotection by glycine betaine through adjustment of its bio-catalytic machinery*

To further investigate the influence of salt stress and glycine betaine on cellular physiology under conditions of carbon limitation, we determined the absolute concentrations of 39 proteins and protein complex subunits of central carbon metabolism and of the proline synthesis pathway using the QconCAT technology (see *Experimental Procedures*). We observed that the intracellular abundance of the studied proteins differed substantially. Citrate synthase (CitZ), isocitrate dehydrogenase (Icd), malate dehydrogenase (Mdh) and glutamine synthetase (GlnA) were among the most abundant proteins under all conditions. The three TCA cycle enzymes form a protein complex that may be involved in substrate channeling through this pathway (Meyer *et al.*, 2011; Bartholomae *et al.*, 2014). Concerning the enzymes of the anabolic and osmostress-adaptive proline synthesis, the dual-purpose enzyme ProA (Brill *et al.*, 2011a) showed a higher abundance than all other proteins of this pathway under all conditions.

Similar to what has been observed before for proteome and transcriptome analyses with *B. subtilis* (Chubukov *et al.*, 2013), salt stress had a pronounced effect on the cellular protein levels that went far beyond what was expected from the inspection of the transcriptome profile of salt-stressed cells. The presence of 1.2 M NaCl triggered an increase in intracellular levels of the majority of the analysed proteins (Fig. 5). This included mainly the enzymes of the Embden-Meyerhof-Parnas pathway and TCA cycle down to the node of 2-oxoglutarate, such as phosphoglucoisomerase (Pgi), phosphoglycerate mutase (Pgm), fructose 1,6-bisphosphate aldolase (FbaA), glyceraldehyde 3-phosphate dehydrogenase (GapA), the pyruvate dehyrogenase complex (PdhCD), and isocitrate dehydrogenase (Icd). The increased expression of glycolytic genes may at least partially result from the increased glucose uptake in salt-stressed cells (see Table 1). In contrast, subunits and proteins of the part of the TCA cycle downstream of 2-oxoglutarate dehydrogenase were present in reduced amounts, a finding that perfectly matches with the re-routing of substrate flux from the TCA cycle towards the osmoprotectant proline (Fig. 3B). Examples of this trend are succinyl-CoA synthetase (SucCD), succinate dehydrogenase (SdhBC),
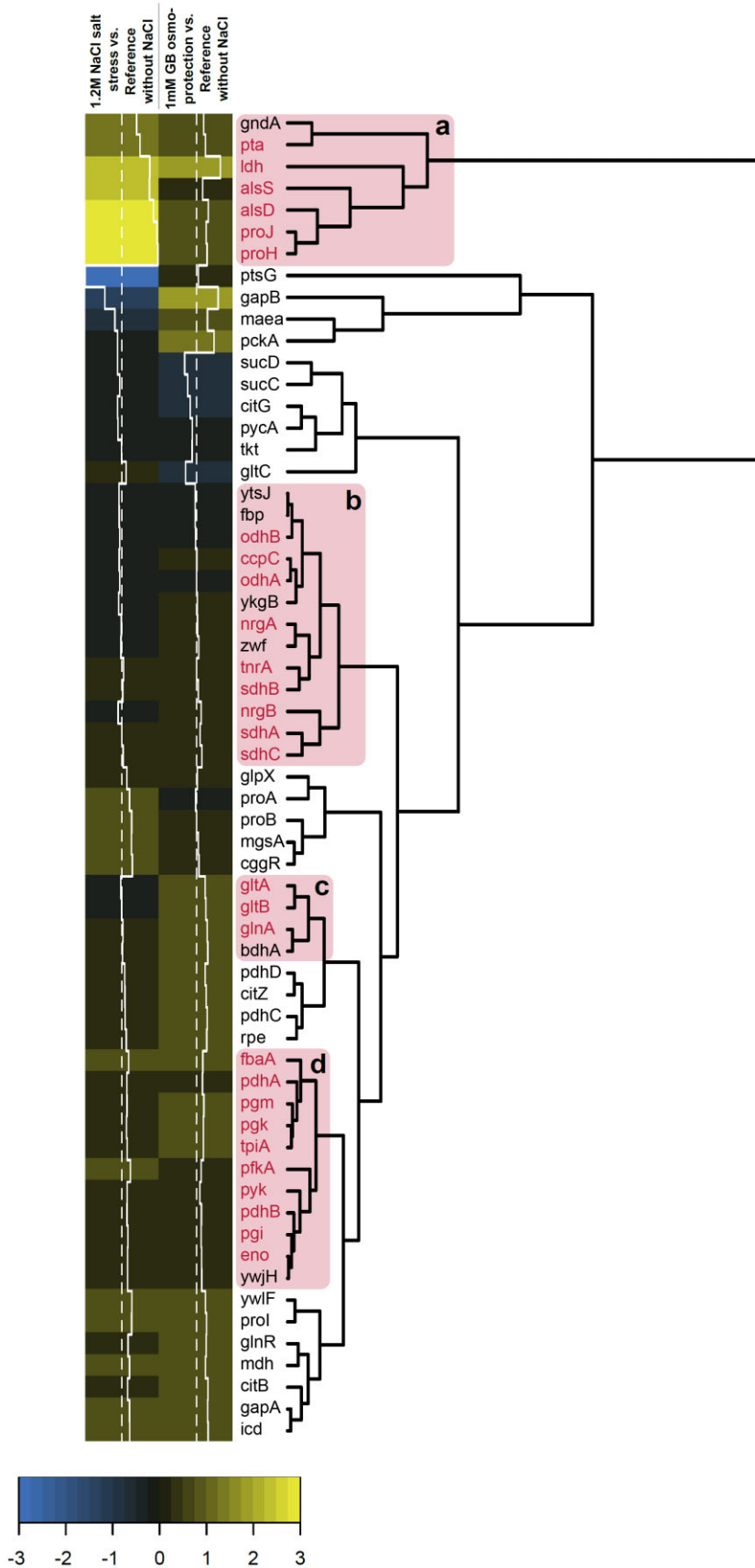
Fig. 4. Hierarchical cluster analysis of gene expression of 61 genes in carbon core metabolism, glucose uptake, glutamine, glutamate and proline metabolism (selected according to SubtiWiki database version 2013/2). Four functional branches can be identified containing mainly:
A. Genes of osmosensitive proline synthesis.
B. Genes belonging to ammonium metabolism and citric acid cycle.
C. Genes involved in glutamate synthesis.
D. Genes coding for glycolytic enzymes.
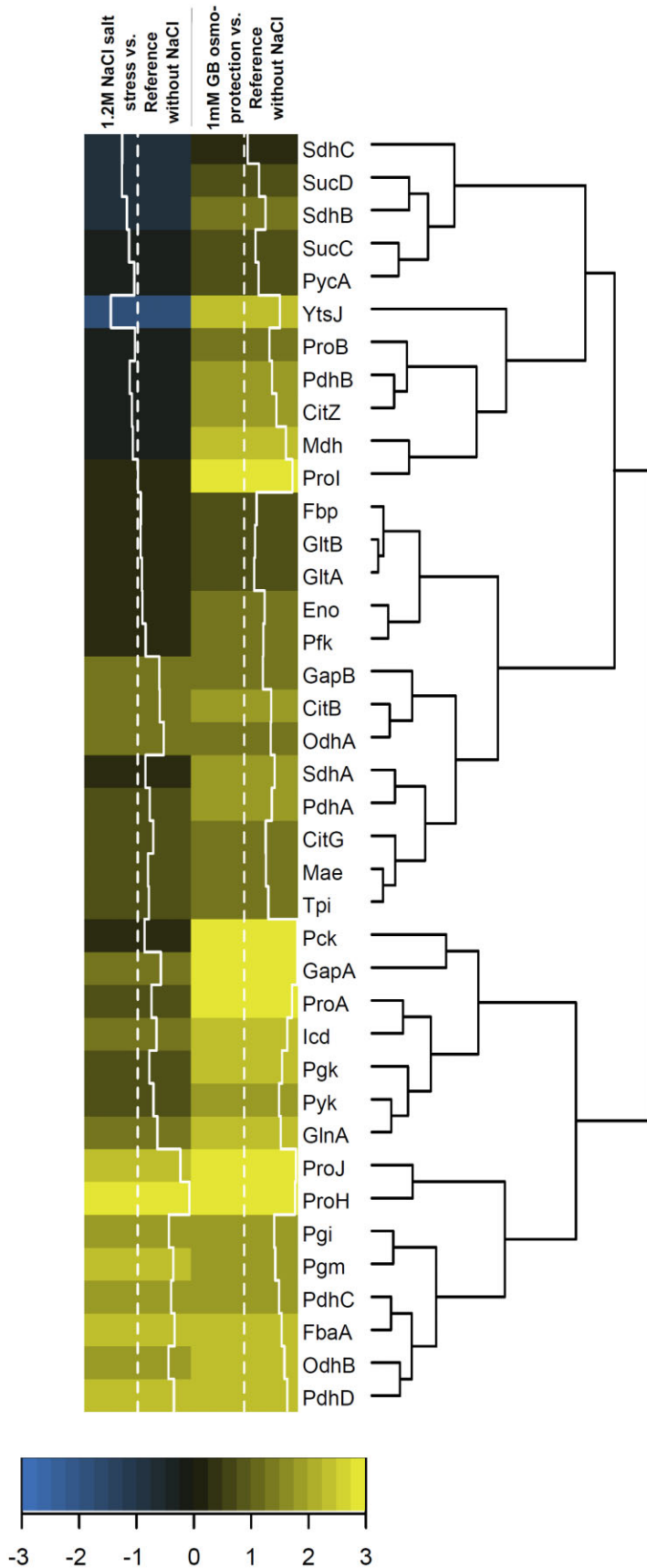Red coloration of gene names indicates functionally related genes within a cluster.

Fig. 5. Hierarchical cluster analysis of expression of 39 proteins and protein complex subunits of carbon core metabolism and proline metabolism.

Table 3. Specific activity of enzymes from carbon core metabolism of *B. subtilis* grown in M9 medium.

	Condition							
	Reference		600 mM K$^+$		Salt stress		Osmoprotection	
Enzyme	300 mM KCl, 25 mM proline		600 mM KCl		600 mM KCl, 500 mM proline		600 mM KCl, 25 mM proline, 650 mM glycine betaine	
Glucose 6-phosphate isomerase	2.101	± 0.009	1.387	± 0.031	1.233	± 0.017	1.798	± 0.023
Fructose 1,6-bisphosphate aldolase	0.049	± 0.003	0.030	± 0.003	0.030	± 0.003	0.051	± 0.006
Pyruvate kinase	0.231	± 0.014	0.191	± 0.000	0.191	± 0.000	0.183	± 0.014
Glucose 6-phosphate dehydrogenase	0.375	± 0.003	0.302	± 0.009	0.301	± 0.010	0.315	± 0.009
6-phosphogluconate dehydrogenase	0.205	± 0.010	0.090	± 0.005	0.103	± 0.010	0.151	± 0.010
Citrate synthase	0.141	± 0.005	0.089	± 0.004	0.101	± 0.014	0.120	± 0.019
Isocitrate dehydrogenase	1.640	± 0.031	1.140	± 0.020	1.199	± 0.004	1.406	± 0.039
Malate dehydrogenase	0.561	± 0.054	0.585	± 0.028	0.519	± 0.042	0.670	± 0.031
Fructose 1,6-bisphosphatase	0.203	± 0.008	0.116	± 0.012	0.107	± 0.002	0.184	± 0.005
Malic enzyme	0.009	± 0.003	0.015	± 0.006	0.018	± 0.003	0.018	± 0.003

The assay mixture was untreated for the reference, and amended with effectors to mimic salt stress (600 mM KCl, 500 mM proline) and osmoprotection (600 mM KCl, 25 mM proline, 650 mM glycine betaine). The effector concentrations were chosen according to (Hoffmann *et al.*, 2013) and (Whatmore *et al.*, 1990). In addition, the effect of potassium ions alone was studied by addition of 300 mM and 600 mM KCl. All experiments are carried out in triplicates ($n = 3$). The enzyme activity is given in μmol min^{-1} (mg protein)$^{-1}$.

malate dehydrogenase (Mdh) and the NADP-dependent major malic enzyme (YtsJ) (Fig. 5). The levels of many of the monitored proteins further increased when glycine betaine was added to the salt-stressed cells (Fig. 3B and 5). This effect was most pronounced for the TCA cycle protein complex CitZ-Icd-Mdh, the gluconeogenic enzymes (PckA, GapB) and the anabolic proline synthesis pathway (ProA, ProB, ProI), but occurred also for other proteins such as SucCD, SdhABC and PdhAB and the glycolytic enzymes. Interestingly, the change in the amount of protein complex subunits was not always stoichiometric. For instance, whereas the quantity of subunit PdhA and PdhB of the pyruvate dehydrogenase complex was not affected by salt stress, the two remaining subunits PdhC and PdhD showed an about fourfold increase, suggesting that the original protein complex stoichiometry under reference conditions is not necessarily maintained. SdhABC was affected in a similar manner. Despite the reduced requirement for osmostress-adaptive *de novo* proline synthesis via the ProJ-ProA-ProH route in cells grown in the presence of glycine betaine (Brill *et al.*, 2011a; Hoffmann *et al.*, 2013), ProJ and ProH were present in the same quantities in stressed cells and cells protected by glycine betaine.

Increase in protein amounts compensates for salt-dependent inhibition of their catalytic activity

At a first glance, the homeostatic flux state of many of the biochemical conversions in carbon core metabolism (Fig. 3B and C) seemed to be in contradiction to the strongly increased level of many of the involved enzymes (Fig. 5). However, salt-stressed cells of *B. subtilis* exhibit not only elevated levels of proline (Fig. 3A), but also increases in their potassium pool (Whatmore *et al.*, 1990). This obviously provides an altered chemical environment (Wood, 2011), and these changes could therefore potentially impact the functioning of many enzymes. To study such potential effects in more detail, we carried out activity assays of a selected set of enzymes under *in vitro* conditions that might mimic the three different *in vivo* scenarios studied in this work (Table 3). Elevated potassium levels significantly reduced the catalytic activity of enzymes of all pathways of central carbon metabolism (see Table 3). This observation implies a reduced catalytic efficiency of many carbon core metabolic enzymes in salt-stressed *B. subtilis* cells. Obviously, the cell partially compensates for the reduced enzyme activities by producing more of these enzymes (Fig. 5). Reduction in enzyme activity was even observed when large amounts of the compatible solute proline were included in the enzyme assays. In contrast to proline, glycine betaine partially restored the original enzyme activity levels (Table 3). This observation may be explained by previous reports that glycine betaine is a better osmoprotectant than proline and affects the solvent properties of the cytoplasm in a way different from that afforded by proline (Cayley and Record, 2003; Wood, 2011).

Discussion

In its natural environments, the soil, plant surfaces and marine sediments, *B. subtilis* is exposed to a wide variety of stress conditions, such as nutrient limitations, challenging temperatures, pH values and osmotic conditions. Numerous studies have addressed the cellular response
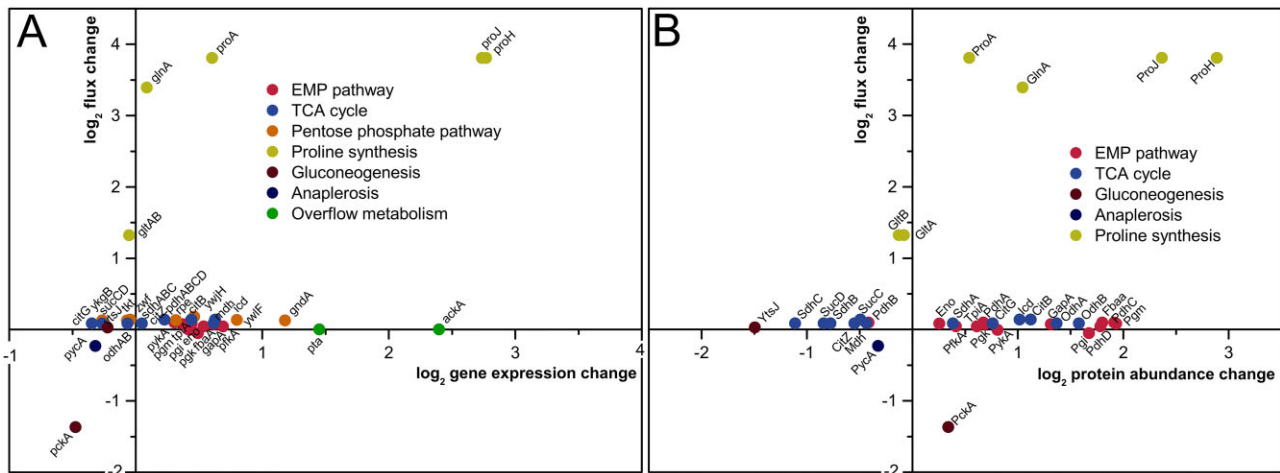
Fig. 6. A. Correlation of the change of metabolic flux to the change in the expression level of the encoding gene.
B. Abundance of the catalysing protein between salt-stressed and non-stressed *B. subtilis*.
For the correlation, NADP-dependent YtsJ was considered as sole active malic enzyme (Lerondel *et al.*, 2006). ProH and ProJ were regarded as the active pathway enzymes under osmotic stress (Brill *et al.*, 2011a).

to individual stress factors and the molecular mechanisms that govern these adaptation processes (Hecker *et al.*, 2007; Nicolas *et al.*, 2012). However, in nature *B. subtilis* frequently faces multiple stresses simultaneously: complex and intertwined adaptive responses of the cell can therefore be foreseen. Here, we present a multi-omics study of the response of *B. subtilis* to different simultaneously imposed stress conditions, a set-up that might more closely reflect the nutrient-limited growth of cells in natural ecosystems. For this purpose, we have developed an experimental approach that utilizes carefully chosen growth conditions in chemostats and that allowed us to analyse the system-wide response of *B. subtilis* to simultaneous carbon limitation and salt stress as two common determinants of bacterial physiology (Bernhardt *et al.*, 2003; Bremer, 2003; Earl *et al.*, 2008; Otto *et al.*, 2010).

Both challenges require complex cellular adaptation processes. Under conditions of carbon limitation, the cell has to route the central carbon and energy metabolism in a way that sufficient precursors and reducing power for anabolism as well as energy are produced (Bernhardt *et al.*, 2003; Koburger *et al.*, 2005; Tännler *et al.*, 2008; Buescher *et al.*, 2012; Nicolas *et al.*, 2012). On the other hand, the protection against osmotic stress requires the massive synthesis of the compatible solute proline to counteract the efflux of water from the cell (Whatmore *et al.*, 1990; Brill *et al.*, 2011a; Hoffmann *et al.*, 2013). A thorough understanding of the anticipated complex response of cells faced with these two stresses at the same time required the application of a systems biology approach in which we integrated metabolomic, fluxomic,

transcriptomic and proteomic analyses into a carefully curated dataset.

A central finding of our study is the robustness of the operation of central carbon metabolism, i.e. the fluxome, under the three conditions considered here. Our observation is in excellent agreement with previous reports of stability of central metabolic processes in *B. subtilis* (Fischer and Sauer, 2005; Schilling *et al.*, 2007; Chubukov *et al.*, 2013). However, the data presented here go beyond concluding robustness – they demonstrate how this robustness in cellular metabolism is achieved by adjusting multiple important checkpoints at the metabolome, transcriptome and proteome levels. This is exemplified here for the central metabolic pathways Embden-Meyerhof-Parnas pathway, pentose phosphate pathway and the TCA cycle. The amounts of the corresponding enzymes of these critical pathways differ substantially under the three conditions (see Figs. 2 and 3). For example, several glycolytic enzymes such as phosphoglucoisomerase, fructose 1,6-bisphosphate aldolase and phosphoglycerate mutase strongly accumulate under salt stress conditions. Yet, the concentrations of main glycolytic intermediates remained unaffected thereby resulting in a constant flux. This apparent imbalance between enzyme concentrations and fluxes (see Fig. 6) appears surprising at a first glance. However, this picture becomes clearer by considering the solvent properties of the cytoplasm (Wood, 2011) under the different stress conditions. Upon the imposition of osmotic stress, the cell rapidly imports large amounts of potassium as an emergency reaction, whose pool size is subsequently reduced again through the massive synthesis of proline

and export of potassium (Whatmore *et al.*, 1990; Holtmann *et al.*, 2003; Brill *et al.*, 2011a). The close inspection of the enzyme properties in an *in vitro* setup mimicking the cellular conditions revealed that the activity of most studied enzymes decreases with elevated potassium concentrations. In most cases, enzyme activity cannot be recovered by adding high concentrations of proline to the assay mixture (see Table 3). Thus, increased production of enzymes under salt stress conditions (Figs. 2 and 5) compensates for their reduced specific activity and is needed to sustain flux homeostasis. It is well established that glycine betaine is a better osmoprotectant than proline (Cayley *et al.*, 1992; Hoffmann *et al.*, 2013). Indeed, the addition of glycine betaine to the enzyme assays largely rescued the enzyme activities from inhibition by salt (see Table 3). This protective effect of glycine betaine might contribute significantly to its superiority as an osmoprotectant for *B. subtilis* in comparison with proline (Zaprasis *et al.*, 2013). The adjustment of the biocatalytic machinery comprises also complex changes in the transcriptional profile of the corresponding genes (see Fig. 6). To the best of our knowledge, this is the first study that traces the relation between the robustness of the metabolic network and the adaptation at the transcriptome and proteome levels back to the direct activities of the enzymes that are at the heart of metabolism.

Under conditions of severe osmotic stress, metabolism is re-routed to the synthesis of huge amounts of the compatible solute proline, whose pool size can reach 0.5 M in severely osmotically stressed cells (e.g., with 1.2 M NaCl) (Whatmore *et al.*, 1990; Hoffmann *et al.*, 2013) (see Fig. 2A). Our data explain how this is achieved. In agreement with previous studies, this involves the induction of the salt-responsive proline biosynthetic *proHJ* operon and the sustained expression of *proA* (Brill *et al.*, 2011a) (see Fig. 2A). Moreover, our data document the accumulation of the corresponding enzymes of this biosynthetic pathway under conditions of osmostress (see Fig. 6B). The enhanced mRNA transcript and enzyme levels account for the observed increased flux towards proline during salt stress (see Fig. 3).

The general robustness of central metabolic fluxes seems to be counter-intuitive with respect to the accumulation of proline to very substantial levels under osmostress conditions. However, a closer view shows that only a small fraction of the total flux is withdrawn from the TCA cycle towards glutamate production and proline biosynthesis. This flux redirection is supported by downregulation of the part of the TCA cycle downstream from succinyl-CoA (Fig. 2A). Moreover, expression of the major catabolic glutamate dehydrogenase RocG (Belitsky and Sonenshein, 1998; Commichau *et al.*, 2008) is downregulated during salt stress. In addition, the glutamine synthetase GlnA accumulates under these conditions resulting in a higher demand for glutamate. Thus, the concerted action of multiple steps around the 2-oxoglutarate node ensures that the cellular equilibrium between 2-oxoglutarate and glutamate can be significantly shifted towards glutamate, which is the starting point for proline biosynthesis (Figs. 2A and 3). We also observed increased amounts of the subunits of the 2-oxoglutarate dehydrogenase complex, OdhA, OdhB, and PdhD (Meyer *et al.*, 2011). This upregulation may counteract a possibly reduced stability of the complex in the presence of salt.

A rather surprising observation is the high-level transcription of the catabolic *putBCP* operon and the sustained production of the PutB and PutC proline catabolic enzymes under conditions of osmotic stress (see Fig. 2A). This might be a consequence of limiting carbon supply in the chemostat which relieves catabolite repression (Singh *et al.*, 2008) and might prompt the cells to exploit alternative nutritional sources. Another trigger might be leakage of proline from salt-stressed cells, thus ensuing PutR-mediated induction of the *putBCP* operon (Hoffmann *et al.*, 2012; Moses *et al.*, 2012).

Our multi-omics approach provides a complex picture of the cellular adjustment of *B. subtilis* to dual stress conditions. The integrated inspection of the various omics datasets reveals a link between the different cellular components during stress response (see Fig. 6). Particularly, flux homeostasis was achieved by a complex rearrangement of transcript and protein levels. To exploit these correlations further, we performed a canonical correlation analysis (Lê Cao *et al.*, 2009). This unsupervised statistical approach identified three intuitive clusters of metabolites and transcripts that are co-regulated during stress responses under simultaneous constrains in carbon supply and challenges by high salinity (Fig. 7). The first group (marked in yellow) contains proline, glutamine and fumarate in association with genes involved in glutamate synthesis (*glnA*, *gltAB*) and gluconeogenesis (*pckA*, *gapB*), and is thus central to providing precursors for synthesis of the osmoprotectant proline. In addition, proline biosynthesis itself is part of a larger, pathway-overspanning cluster. This second group (marked in red) contains compounds of lower glycolysis and of the entrance into the TCA cycle (3-phosphoglycerate, phosphoenolpyruvate, pyruvate, citrate) and it clusters with genes for proline synthesis and degradation (*proA*, *proB*, *proH*, *proJ*, *putB*, *putC*, *putP*). Finally, the third cluster (marked in blue) comprises energy metabolites (ATP, GTP) and different intermediates of central carbon metabolic pathways (fructose 1,6-bisphosphate, acetyl-CoA, erythrose 4-phosphate, ribose 5-phosphate and malate) and transcripts of the anaplerotic pyruvate carboxylase *pycA* and fumarase *citG*. These clear correlations thus

Fig. 7. Two-dimensional loading plot of regularized canonical correlation analysis reveals regulatory associations between metabolites and transcripts in central metabolism. Three groups of associations can be identified: the first group shown in yellow contains proline, glutamine and fumarate in association with genes involved in ammonium utilization (*glnA*, *gltAB*) and gluconeogenesis (*pckA*, *gapB*); the second group shown in red contains compounds of lower glycolysis and of the entrance into TCA cycle (3PG, PEP, PYR, CIT) clustering with genes of proline synthesis and degradation (*proA*, *proB*, *proH*, *proJ*, *putB*, *putC*, *putP*); the third group shown in blue contains cofactors (ATP, GTP) and different intermediates of EMP, PPP and TCA cycle (F1,6BP, Acetyl-CoA, E4P, R5P, MAL) clustering with anaplerotic pyruvate carboxylase *pycA* and fumarase *citG*; Components in green are regulatory related and form less pronounced clusters.

substantiate our main conclusion that the cell recruits metabolic modules across individual pathways in order to achieve both a robust metabolism and appropriate metabolic responses to stress conditions.

The overall picture that emerges from our analysis, i.e. increased and decreased amounts of enzymes of the central metabolic pathways upstream and downstream of the 2-oxoglutarate node, is in accordance with previous proteome studies of salt-shocked *B. subtilis* cells (Höper *et al.*, 2006; Otto *et al.*, 2010). However, our integrated analysis of the proteome, the fluxome and of enzyme-specific activities goes far beyond these initial observations and provides a system-level explanation for the observed effects of salt stress. Homeostasis relies on global adaptations of cellular components, and the response to the imposed stress is not simply the sum of individual changes. Concerted responses to nutritional and environmental challenges obviously require the functional network as a whole.

Experimental procedures

Strain and growth conditions

Experiments were performed with the prototrophic *B. subtilis* strain BSB1 (168 Trp⁺) (Nicolas *et al.*, 2012). For pre-

cultures, complex Luria–Bertani (LB) medium containing 10 g l⁻¹ of tryptone (BD Biosciences, Heidelberg, Germany), 5 g l⁻¹ of yeast extract (BD Biosciences) and 10 g l⁻¹ of NaCl was used. For plating of cells, the medium was supplemented with 15 g l⁻¹ of agar (Sigma-Aldrich, Steinheim, Germany). Subsequent cultivations were performed in minimal M9 medium with glucose as sole carbon source at 5 g l⁻¹ (second pre-culture) and 1 g l⁻¹ (main culture) respectively. The medium also contained per liter: 8.5 g of $Na_2HPO_4 \cdot 2H_2O$, 3 g of KH_2PO_4, 1 g of NH_4Cl, 0.5 g of NaCl, 246 mg of $MgSO_4 \cdot 7H_2O$, 30 mg of 3,4-dihydroxybenzoate, 14.7 mg of $CaCl_2 \cdot 2H_2O$, 13.5 mg of $FeCl_3 \cdot 6H_2O$, 1.7 mg of $ZnCl_2$, 1 mg of $MnCl_2 \cdot 4H_2O$, 0.43 mg of $CuCl_2 \cdot 2H_2O$, 0.6 µg of $CoCl_2 \cdot 6H_2O$ and 0.6 µg of $Na_2MoO_4 \cdot 2H_2O$. It was supplemented with 70.13 g l⁻¹ NaCl (1.2 M, corresponding to 2560 mosm kg⁻¹) with or without 117.15 mg l⁻¹ of glycine betaine (1 mM) to mimic osmotic stress conditions and the osmoprotection of *B. subtilis* cells by an externally provided compatible solute respectively. For metabolic flux analysis, naturally labelled glucose was replaced by 99% [1-¹³C] glucose (Euriso-top, Gif sur Yvette, France). All cultivations were conducted at 37°C. First, cells from glycerol stocks were incubated overnight on LB agar. Single colonies were then grown for 2 h (100 ml baffled shake flasks, 10 ml of LB medium, 230 r.p.m.), harvested by centrifugation, washed and used to inoculate the second pre-culture in 50 ml of M9 medium (500 ml baffled shake flasks, 230 r.p.m.). Washed cells, harvested during exponential growth, served as inoculum for continuous cultivation at 0.1 h⁻¹ in a parallelized 1 l bioreactor system with a

working volume of 300 ml, kept at an aeration rate of 9 l h^{-1} and a stirrer speed of 1000 r.p.m. (dasGIP, Jülich, Germany). Culture settings were controlled at 37°C and pH 7.1. For each condition, four biological replicates were conducted. One of these contained the isotopic tracer medium for ^{13}C metabolic flux analysis. One of the reactors was connected to a mass spectrometer (Pfeiffer Vacuum, Asslar, Germany) for exhaust gas analysis. Cultivations were performed until metabolic and isotopic steady state was reached, i.e. for five volume changes. Then, cells were harvested for parallel analysis of the transcriptome, metabolome, proteome and fluxome respectively.

Analysis of cell concentration

Cell concentration was monitored as optical density (OD$_{600}$) at 600 nm (Biochrom Libra Instruments, Cambridge, UK). Dry cell weight (DCW) was determined gravimetrically after filtration of 25 ml culture broth (0.2 μm; Sartorius, Göttingen, Germany), including washing of the cells on the filter with 25 ml of a salt solution that matched the ionic strength of the medium and with deionized water, respectively, and subsequent drying at 80°C to constant weight. The carbon content of dried biomass pellets was determined by elemental analysis (Elementar Analysensysteme GmbH, Hanau, Germany).

Transcriptome analysis

Cells were harvested as described previously (Winter *et al.*, 2011). Total RNA was extracted by mechanical cell disruption followed by organic extraction with acid phenol (Eymann *et al.*, 2002). Transcriptome analysis was conducted using an Agilent (Waldbronn, Germany) custom microarray (Winter *et al.*, 2011). As the analysis was performed by hybridizing individual samples against a common reference, the values obtained represent relative gene expression levels at a given time point. Microarray data have been deposited in the NCBI's Gene Expression Omnibus (GEO) database and are accessible through GEO Series accession no. GSE53333. A detailed protocol is provided in the supplement (Supporting Information Appendix S2).

Proteome analysis – assay development for targeted protein quantification

Multiplex quantification of proteins was accomplished by combining proteotypic peptides into quantification concatamers (QconCats) (Beynon *et al.*, 2005). The QconCAT proteins used in this study covered enzymes of the central carbon metabolism, and the glutamate and proline biosynthetic pathways of *B. subtilis.* Design of the QconCAT proteins was performed according to commonly accepted guidelines (Pratt *et al.*, 2006). Three proteotypic peptides (PTPs) were selected for each protein of interest of which at least two peptides were used for the protein quantification (see Supporting Information Table S1). PTPs were selected based on the highest sequest X-corr values obtained from datasets previously measured in-house (Otto *et al.*, 2010). For proteins and peptides, never found in the in-house measurement, theoretic tryptic peptides were selected. Collision

energy and retention time for each of the PTPs (using pure QconCAT purchased from Polyquant GmbH, Bad Abbach, Germany) were optimized using Skyline (v1.3, MacCoss Lab Software, Seattle, WA, USA) on a triple quadrupole mass spectrometer (TSQ Vantage, Thermo Scientific, Bonn, Germany) operated in single reaction monitoring (SRM) mode. For ionization, 1800 V of spray voltage and 250°C capillary temperature were used. The resolution for both quadrupoles, Q1 and Q3 was set to 0.7 Da. The collision gas pressure of Q2 was set at 1.5 mTorr. Peptide separation was carried out using an Acelaim PepMap 100 column (C$_{18}$, 3 mm, 100 Å, 15 cm bed length; Dionex, Idstein, Germany) and a binary gradient from 0% to 40% buffer B (100% acetonitrile [v/v], 0.1% acetic acid [v/v]) in 70 min and to 100% B in additional 15 min at a flow rate of 300 nl min^{-1}. Following the parameter optimization, three transitions (product ions) per peptide (precursor) with top three ranked intensities were chosen for targeted analysis. A scheduled multiple reaction monitoring (MRM) method with maximum 2 s of cycle time and a retention time window of ± 2.5 min was created using the retention time recorded during parameter optimization.

Proteome analysis – sample preparation and data analysis

Briefly, protein extracts from frozen pellets were prepared and analysed as described previously (Maaß *et al.*, 2011). Appropriate amounts of QconCATs were spiked into 15 μg of protein extract. Samples were separated on NuPAGE® Bis-Tris Gels 4–12% (Life Technologies Corporation, Carlsbad, CA, USA) for 5 min to isolate the proteins of interest from contaminants, otherwise interfering with subsequent processing. Staining and de-staining was carried out according to the manufacturer's guidelines. Subsequently, each lane was cut into three pieces and digested with trypsin (Promega, Madison, WI, USA) overnight (16 h) at 37°C (Thiele *et al.*, 2007). Purified tryptic peptides were then pooled and used for analysis by MRM (Picotti and Aebersold, 2012). Two liquid chromatography tandem mass spectrometry (LC-MS/MS) measurements were performed for each sample. The raw data files were analysed by Skyline (MacLean *et al.*, 2010). The resulting ratios from peak areas for endogenous light peptides to heavy Qpeptides were exported. Based on the known amount of the spiked Qpeptides, the endogenous light peptide concentrations were calculated. Peptides that exhibited missed cleavage and insufficient chromatographic properties, respectively, were excluded from quantification of the corresponding protein. A detailed protocol is provided in the supplement (Supporting Information Appendix S3, Fig. S1).

Metabolome analysis

Samples for intracellular metabolome analysis were obtained by an extended fast vacuum dependent filtration (Meyer *et al.*, 2010). After filtration (0.45 μm; S-Pak, Merck Millipore, Billerica, MA, USA), filters with cells were transferred into the extraction solution (60% ethanol, < 4°C). The entire sample was immediately frozen in liquid nitrogen. Prior to metabolite extraction and cell disruption, internal standards were added to a final concentration of 20 nmol (ribitol and norvaline for gas chromatography mass spectrometry, GC-MS) and

2.5 nmol (camphorsulfonic acid for liquid chromatography mass spectrometry, LC-MS) respectively. Ion pairing LC-MS was used to analyse intracellular nucleosides, nucleotides, sugar phosphates and co-factors. The measurement was conducted on a high-performance liquid chromatography (HPLC) system (1100 series, Agilent Technologies), coupled to a mass spectrometer (micrOTOF, Bruker Daltonics, Bremen, Germany) as described (Liebeke *et al.*, 2010). Metabolite quantification was done with the QuantAnalysis software package (Bruker Daltonics, Bremen, Germany). Intracellular organic acids and glycolytic intermediates were analysed by GC-MS (GC 7890A, inert MSD 5979C, Agilent Technologies) (Liebeke *et al.*, 2008). Metabolite quantification was conducted with the ChomaTOF software (LECO, St. Joseph, MI, USA). Intracellular amino acids were harvested via vacuum filtration and quantified via HPLC as described previously by Krömer and colleagues (2005). The extracellular metabolome was analysed from filtrates of 2 ml of culture supernatants (0.2 μm, Filtropur S, Sarstedt, Germany) by ^{1}H-NMR (Liebeke *et al.*, 2011). Nuclear magnetic resonance (NMR) spectra were obtained at 600.27 MHz and a temperature of 37°C (Bruker AVANCE-II 600, Bruker Biospin GmbH, Rheinstetten, Germany), and data analysis was done with the AMIX software (Bruker Biospin). The signal area of the internal standard trimethylsilyl propanoic acid was used for direct quantification. More specifically, extracellular glucose was quantified enzymatically (YSI Life Sciences, Yellow Springs, OH, USA). Additional parameters are provided in the supplement (Supporting Information Appendix S4). Organic acids and alcohols in the supernatant, i.e. citrate, 2-oxoglutarate, pyruvate, succinate, lactate, formate, acetate, acetoin, isobutyrate, ethanol and isovalerate, were monitored by HPLC equipped with an ion exchange column (Aminex HPX-87H, Bio-Rad, Hercules, CA, USA), isocratic elution with 12 mM H_2SO_4 at a flow rate of 0.5 ml min^{-1} and 45°C, and detection by UV absorbance (210 nm) and refractive index (Hitachi, Tokyo, Japan).

Fluxome analysis

Intracellular carbon fluxes were determined with the software OpenFLUX (Quek *et al.*, 2009). All calculations were performed in Matlab 7.2 (The Mathworks, Natick, MA, USA). The metabolic model of *B. subtilis* was derived from primary literature (Dauner and Sauer, 2001; Oh *et al.*, 2007; Goelzer *et al.*, 2008) and the SubtiWiki database (Mäder *et al.*, 2012) and included all major pathways carbon core metabolism as well as proline and glutamate synthesis (see Supporting Information Table S2). Based on a comprehensive approach of metabolite and isotopomer profiling, the fluxes were derived by minimization of the sum of the weighted least-square residuals between the measured and the simulated ^{13}C labelling patterns (see Supporting Information Table S3) respectively. All measured extracellular fluxes (Table 1) and anabolic fluxes into biomass were taken into account (see Supporting Information Table S4). The ^{13}C labelling analysis of proteinogenic amino acids from hydrolysed cell protein was performed by GC-MS (GC 7890A, inert MSD 5979C, Agilent Technologies) (Bolten *et al.*, 2009), including *t*-butyl-dimethylsilyl derivatization (Krömer *et al.*, 2008). The observed mass isotopomer distributions were corrected for

natural isotopes (van Winden *et al.*, 2002). Fluxes into biomass were calculated from the known macromolecular composition of the cell (Dauner and Sauer, 2001; Oh *et al.*, 2007). The latter was corrected for the influence of high salinity on *Bacillus*, particularly changes in the content of protein, ions, intracellular amino acids, as well as the content and composition of the cell wall (Dartois *et al.*, 1998; López *et al.*, 1998; 2006), as given in the supplement (see Supporting Information Table S4). Subsequent Monte-Carlo analysis provided 90% confidence intervals for the estimated flux parameters (Wittmann, 2002).

Enzyme activity assays

Cells were harvested, re-suspended in Tris/HCl buffer and disrupted in a bench-top homogenizer (MP Biomedicals, Santa Ana, CA, USA). The molarity and pH value of the buffer varied for each enzyme, depending on its specification, as given in the corresponding references. The activity of glucose 6-phosphate dehydrogenase (Moritz *et al.*, 2000), phosphoglucoisomerase, 6–phosphogluconate dehydrogenase, fructose 1,6-bisphosphatase (Dominguez *et al.*, 1998), fructose bisphosphate aldolase (Engels *et al.*, 2008), pyruvate kinase (Netzer *et al.*, 2004), citrate synthase (Radmacher and Eggeling, 2007), isocitrate dehydrogenase (Becker *et al.*, 2009), malate dehydrogenase (Yoshida, 1965) and malic enzyme (Lerondel *et al.*, 2006) was assayed by spectrophotometry (Specord 40, Analytik Jena, Jena, Germany). The total protein content of the cell extracts was determined with a BCA protein assay kit (Thermo Scientific, Rockford, IL, USA).

Statistical analysis and visualization of multi-omics datasets

Multi-omics datasets were integrated and visualized by the software ProMeTra (Bielefeld, Germany; Neuweger *et al.*, 2009). Flux visualization was performed by the tool VANTED (Gatersleben, Germany; Junker *et al.*, 2006), including the FluxMap add-on (Rohn *et al.*, 2012). Hierarchical clustering, principle component analysis and canonical correlation analysis were performed with R using the packages gplots (Warnes *et al.*, 2013), FactoMineR (Lê *et al.*, 2008) and mixOmics (Lê Cao *et al.*, 2009) respectively. Hierarchical cluster analysis of gene expression (Figs. 4 and 5) was performed using Euclidean distance and complete linkage as measure of distance and dissimilarity. Data were averaged over all replicates and log$_2$ transformed prior to analysis. Analysis of regulons and functional assignments of genes were derived from the SubtiWiki database (Mäder *et al.*, 2012).

References

Atkinson, D.E. (1968) Energy charge of the adenylate pool as a regulatory parameter. Interaction with feedback modifiers. *Biochemistry* **7:** 4030–4034.

Bartholomae, M., Meyer, F.M., Commichau, F.M., Burkovski, A., Hillen, W., and Seidel, G. (2014) Complex formation between malate dehydrogenase and isocitrate dehydrogenase from *Bacillus subtilis* is regulated by tricarboxylic acid cycle metabolites. *FEBS J* **281:** 1132–1143.

Becker, J., Klopprogge, C., Schröder, H., and Wittmann, C. (2009) Metabolic engineering of the tricarboxylic acid cycle for improved lysine production by *Corynebacterium glutamicum*. *Appl Environ Microbiol* **75:** 7866–7869.

Belitsky, B.R., and Sonenshein, A.L. (1998) Role and regulation of *Bacillus subtilis* glutamate dehydrogenase genes. *J Bacteriol* **180:** 6298–6305.

Bernhardt, J., Weibezahn, J., Scharf, C., and Hecker, M. (2003) *Bacillus subtilis* during feast and famine: visualization of the overall regulation of protein synthesis during glucose starvation by proteome analysis. *Genome Res* **13:** 224–237.

Beynon, R.J., Doherty, M.K., Pratt, J.M., and Gaskell, S.J. (2005) Multiplexed absolute quantification in proteomics using artificial QCAT proteins of concatenated signature peptides. *Nat Methods* **2:** 587–589.

Boch, J., Kempf, B., and Bremer, E. (1994) Osmoregulation in *Bacillus subtilis*: synthesis of the osmoprotectant glycine betaine from exogenously provided choline. *J Bacteriol* **176:** 5364–5371.

Bolten, C.J., Heinzle, E., Müller, R., and Wittmann, C. (2009) Investigation of the central carbon metabolism of *Sorangium cellulosum*: metabolic network reconstruction and quantification of pathway fluxes. *J Microbiol Biotechnol* **19:** 23–36.

Bremer, E. (2003) Adaptation to changing osmolarity. In *Bacillus subtilis and Its Closest Relatives*. Sonenshein, A.L., Hoch, J.A., and Losick, R. (eds). Washington, DC, USA: ASM Press, pp. 385–391.

Bremer, E., and Krämer, R. (2000) Coping with osmotic challenges: osmoregulation through accumulation and release of compatible solutes in cacteria. In *Bacterial Stress Responses*. Storz, G., and Hengge-Aronis, R. (eds). Washington, DC, USA: ASM Press, pp. 79–97.

Brill, J., Hoffmann, T., Bleisteiner, M., and Bremer, E. (2011a) Osmotically controlled synthesis of the compatible solute proline is critical for cellular defense of *Bacillus subtilis* against high osmolarity. *J Bacteriol* **193:** 5335–5346.

Brill, J., Hoffmann, T., Putzer, H., and Bremer, E. (2011b) T-box-mediated control of the anabolic proline biosynthetic genes of *Bacillus subtilis*. *Microbiology* **157:** 977–987.

Buescher, J.M., Liebermeister, W., Jules, M., Uhr, M., Muntel, J., Botella, E., *et al.* (2012) Global network reorganization during dynamic adaptations of *Bacillus subtilis* metabolism. *Science* **335:** 1099–1103.

Cayley, S., and Record, M.T. (2003) Roles of cytoplasmic osmolytes, water, and crowding in the response of *Escherichia coli* to osmotic stress: biophysical basis of osmoprotection by glycine betaine. *Biochemistry* **42:** 12596–12609.

Cayley, S., Lewis, B.A., and Record, M.T. (1992) Origins of the osmoprotective properties of betaine and proline in *Escherichia coli* K-12. *J Bacteriol* **174:** 1586–1595.

Chubukov, V., Uhr, M., Le Chat, L., Kleijn, R.J., Jules, M., Link, H., *et al.* (2013) Transcriptional regulation is insufficient to explain substrate-induced flux changes in *Bacillus subtilis*. *Mol Syst Biol* **9:** 709.

Commichau, F.M., Gunka, K., Landmann, J.J., and Stülke, J. (2008) Glutamate metabolism in *Bacillus subtilis*: gene expression and enzyme activities evolved to avoid futile cycles and to allow rapid responses to perturbations of the system. *J Bacteriol* **190:** 3557–3564.

Dartois, V., Débarbouillé, M., Kunst, F., and Rapoport, G. (1998) Characterization of a novel member of the DegS-DegU regulon affected by salt stress in *Bacillus subtilis*. *J Bacteriol* **180:** 1855–1861.

Dauner, M., and Sauer, U. (2001) Stoichiometric growth model for riboflavin-producing *Bacillus subtilis*. *Biotechnol Bioeng* **76:** 132–143.

van Dijl, J.M., and Hecker, M. (2013) *Bacillus subtilis*: from soil bacterium to super-secreting cell factory. *Microb Cell Fact* **12:** 3.

Dominguez, H., Rollin, C., Guyonvarch, A., Guerquin-Kern, J.-L., Cocaign-Bousquet, M., and Lindley, N.D. (1998) Carbon-flux distribution in the central metabolic pathways of *Corynebacterium glutamicum* during growth on fructose. *Eur J Biochem* **254:** 96–102.

Earl, A.M., Losick, R., and Kolter, R. (2008) Ecology and genomics of *Bacillus subtilis*. *Trends Microbiol* **16:** 269–275.

Engels, V., Lindner, S.N., and Wendisch, V.F. (2008) The global repressor SugR controls expression of genes of glycolysis and of the L-lactate dehydrogenase LdhA in *Corynebacterium glutamicum*. *J Bacteriol* **190:** 8033–8044.

Eymann, C., Homuth, G., Scharf, C., and Hecker, M. (2002) *Bacillus subtilis* functional genomics: global characterization of the stringent response by proteome and transcriptome analysis. *J Bacteriol* **184:** 2500–2520.

Fillinger, S., Boschi-Muller, S., Azza, S., Dervyn, E., Branlant, G., and Aymerich, S. (2000) Two glyceraldehyde-3-phosphate dehydrogenases with opposite physiological roles in a non-photosynthetic bacterium. *J Biol Chem* **275:** 14031–14037.

Fischer, E., and Sauer, U. (2005) Large-scale *in vivo* flux analysis shows rigidity and suboptimal performance of *Bacillus subtilis* metabolism. *Nat Genet* **37:** 636–640.

Fisher, M.T. (2006) Proline to the rescue. *Proc Natl Acad Sci U S A* **103:** 13265–13266.

Goelzer, A., and Fromion, V. (2011) Bacterial growth rate reflects a bottleneck in resource allocation. *Biochim Biophys Acta* **1810:** 978–988.

Goelzer, A., Bekkal Brikci, F., Martin-Verstraete, I., Noirot, P., Bessières, P., Aymerich, S., and Fromion, V. (2008) Reconstruction and analysis of the genetic and metabolic regulatory networks of the central metabolism of *Bacillus subtilis*. *BMC Syst Biol* **2:** 20.

Gunka, K., and Commichau, F.M. (2012) Control of glutamate homeostasis in *Bacillus subtilis*: a complex interplay between ammonium assimilation, glutamate biosynthesis and degradation. *Mol Microbiol* **85:** 213–224.

Hahne, H., Mäder, U., Otto, A., Bonn, F., Steil, L., Bremer, E., *et al.* (2010) A comprehensive proteomics and transcriptomics analysis of *Bacillus subtilis* salt stress adaptation. *J Bacteriol* **192:** 870–882.

Harwood, C.R. (1992) *Bacillus subtilis* and its relatives: molecular biological and industrial workhorses. *Trends Biotechnol* **10:** 247–256.

Hecker, M., Pané-Farré, J., and Völker, U. (2007) SigB-dependent general stress response in *Bacillus subtilis* and related gram-positive bacteria. *Annu Rev Microbiol* **61:** 215–236.

Hoffmann, T., Blohn, C., Stanek, A., Moses, S., Barzantny, H., and Bremer, E. (2012) Synthesis, release, and recapture of compatible solute proline by osmotically stressed *Bacillus subtilis* sells. *Appl Environ Microbiol* **78:** 5753–5762.

Hoffmann, T., Wensing, A., Brosius, M., Steil, L., Völker, U., and Bremer, E. (2013) Osmotic control of opuA expression in *Bacillus subtilis* and its modulation in response to intracellular glycine betaine and proline pools. *J Bacteriol* **195:** 510–522.

Holtmann, G., Bakker, E.P., Uozumi, N., and Bremer, E. (2003) KtrAB and KtrCD: Two K$^+$ uptake systems in *Bacillus subtilis* and their role in adaptation to hypertonicity. *J Bacteriol* **185:** 1289–1298.

Höper, D., Völker, U., and Hecker, M. (2005) Comprehensive characterization of the contribution of individual SigB-dependent general stress genes to stress resistance of *Bacillus subtilis*. *J Bacteriol* **187:** 2810–2826.

Höper, D., Bernhardt, J., and Hecker, M. (2006) Salt stress adaptation of *Bacillus subtilis*: a physiological proteomics approach. *Proteomics* **6:** 1550–1562.

Junker, B., Klukas, C., and Schreiber, F. (2006) VANTED: a system for advanced data analysis and visualization in the context of biological networks. *BMC Bioinformatics* **7:** 109.

Kempf, B., and Bremer, E. (1998) Uptake and synthesis of compatible solutes as microbial stress responses to high-osmolality environments. *Arch Microbiol* **170:** 319–330.

Koburger, T., Weibezahn, J., Bernhardt, J., Homuth, G., and Hecker, M. (2005) Genome-wide mRNA profiling in glucose starved *Bacillus subtilis* cells. *Mol Genet Genomics* **274:** 1–12.

Kohlstedt, M., Becker, J., and Wittmann, C. (2010) Metabolic fluxes and beyond – systems biology understanding and engineering of microbial metabolism. *Appl Microbiol Biotechnol* **88:** 1065–1075.

Krömer, J.O., Fritz, M., Heinzle, E., and Wittmann, C. (2005) *In vivo* quantification of intracellular amino acids and intermediates of the methionine pathway in *Corynebacterium glutamicum*. *Anal Biochem* **340:** 171–173.

Krömer, J.O., Bolten, C.J., Heinzle, E., Schröder, H., and Wittmann, C. (2008) Physiological response of *Corynebacterium glutamicum* to oxidative stress induced by deletion of the transcriptional repressor McbR. *Microbiology* **154:** 3917–3930.

Lê, S., Josse, J., and Husson, F. (2008) FactoMineR: an R package for multivariate analysis. *J Stat Softw* **25:** 1.

Lê Cao, K.-A., González, I., and Déjean, S. (2009) IntegrOmics: an R package to unravel relationships between two omics datasets. *Bioinformatics* **25:** 2855–2856.

Lerondel, G., Doan, T., Zamboni, N., Sauer, U., and Aymerich, S. (2006) YtsJ has the major physiological role of the four paralogous malic enzyme isoforms in *Bacillus subtilis*. *J Bacteriol* **188:** 4727–4736.

Liebeke, M., Pöther, D.-C., van Duy, N., Albrecht, D., Becher, D., Hochgräfe, F., *et al.* (2008) Depletion of thiol-containing proteins in response to quinones in *Bacillus subtilis*. *Mol Microbiol* **69:** 1513–1529.

Liebeke, M., Meyer, H., Donat, S., Ohlsen, K., and Lalk, M. (2010) A metabolomic view of *Staphylococcus aureus* and Its Ser/Thr kinase and phosphatase deletion mutants: involvement in cell wall biosynthesis. *Chem Biol* **17:** 820–830.

Liebeke, M., Dörries, K., Zühlke, D., Bernhardt, J., Fuchs, S., Pané-Farré, J., *et al.* (2011) A metabolomics and proteomics study of the adaptation of *Staphylococcus aureus* to glucose starvation. *Mol Biosyst* **7:** 1241–1253.

López, C.S., Heras, H., Ruzal, S.M., Sánchez-Rivas, C., and Rivas, E.A. (1998) Variations of the envelope composition of *Bacillus subtilis* during growth in hyperosmotic medium. *Curr Microbiol* **36:** 55–61.

López, C.S., Alice, A.F., Heras, H., Rivas, E.A., and Sánchez-Rivas, C. (2006) Role of anionic phospholipids in the adaptation of *Bacillus subtilis* to high salinity. *Microbiology* **152:** 605–616.

Lopez, D., Vlamakis, H., and Kolter, R. (2009) Generation of multiple cell types in *Bacillus subtilis*. *FEMS Microbiol Rev* **33:** 152–163.

Maaß, S., Sievers, S., Zühlke, D., Kuzinski, J., Sappa, P.K., Muntel, J., *et al.* (2011) Efficient, global-scale quantification of absolute protein amounts by integration of targeted mass spectrometry and two-dimensional gel-based proteomics. *Anal Chem* **83:** 2677–2684.

MacLean, B., Tomazela, D.M., Shulman, N., Chambers, M., Finney, G.L., Frewen, B., *et al.* (2010) Skyline: an open source document editor for creating and analyzing targeted proteomics experiments. *Bioinformatics* **26:** 966–968.

Mäder, U., Schmeisky, A.G., Flórez, L.A., and Stülke, J. (2012) SubtiWiki – a comprehensive community resource for the model organism *Bacillus subtilis*. *Nucleic Acids Res* **40:** D1278–D1287.

Meyer, H., Liebeke, M., and Lalk, M. (2010) A protocol for the investigation of the intracellular *Staphylococcus aureus* metabolome. *Anal Biochem* **401:** 250–259.

Meyer, F.M., Gerwig, J., Hammer, E., Herzberg, C., Commichau, F.M., Völker, U., and Stülke, J. (2011) Physical interactions between tricarboxylic acid cycle enzymes in *Bacillus subtilis*: evidence for a metabolon. *Metab Eng* **13:** 18–27.

Moritz, B., Striegel, K., de Graaf, A.A., and Sahm, H. (2000) Kinetic properties of the glucose-6-phosphate and 6-phosphogluconate dehydrogenases from *Corynebacterium glutamicum* and their application for predicting pentose phosphate pathway flux *in vivo*. *Eur J Biochem* **267:** 3442–3452.

Moses, S., Sinner, T., Zaprasis, A., Stöveken, N., Hoffmann, T., Belitsky, B.R., *et al.* (2012) Proline utilization by *Bacillus subtilis*: uptake and catabolism. *J Bacteriol* **194:** 745–758.

Nannapaneni, P., Hertwig, F., Depke, M., Hecker, M., Mäder, U., Völker, U., *et al.* (2012) Defining the structure of the

general stress regulon of *Bacillus subtilis* using targeted microarray analysis and random forest classification. *Microbiology* **158**: 696–707.

Nau-Wagner, G., Opper, D., Rolbetzki, A., Boch, J., Kempf, B., Hoffmann, T., and Bremer, E. (2012) Genetic control of osmoadaptive glycine betaine synthesis in *Bacillus subtilis* through the choline-sensing and glycine betaine-responsive GbsR repressor. *J Bacteriol* **194**: 2703–2714.

Netzer, R., Krause, M., Rittmann, D., Peters-Wendisch, P., Eggeling, L., Wendisch, V., and Sahm, H. (2004) Roles of pyruvate kinase and malic enzyme in *Corynebacterium glutamicum* for growth on carbon sources requiring gluconeogenesis. *Arch Microbiol* **182**: 354–363.

Neuweger, H., Persicke, M., Albaum, S., Bekel, T., Dondrup, M., Huser, A., *et al.* (2009) Visualizing post genomics datasets on customized pathway maps by ProMeTra – aeration-dependent gene expression and metabolism of *Corynebacterium glutamicum* as an example. *BMC Syst Biol* **3**: 82.

Nicolas, P., Mäder, U., Dervyn, E., Rochat, T., Leduc, A., Pigeonneau, N., *et al.* (2012) Condition-dependent transcriptome reveals high-level regulatory architecture in *Bacillus subtilis*. *Science* **335**: 1103–1106.

Oh, Y.-K., Palsson, B.O., Park, S.M., Schilling, C.H., and Mahadevan, R. (2007) Genome-scale reconstruction of metabolic network in *Bacillus subtilis* based on high-throughput phenotyping and gene essentiality data. *J Biol Chem* **282**: 28791–28799.

Otto, A., Bernhardt, J., Meyer, H., Schaffer, M., Herbst, F.-A., Siebourg, J., *et al.* (2010) Systems-wide temporal proteomic profiling in glucose-starved *Bacillus subtilis*. *Nat Commun* **1**: 137.

Picotti, P., and Aebersold, R. (2012) Selected reaction monitoring-based proteomics: workflows, potential, pitfalls and future directions. *Nat Methods* **9**: 555–566.

Pratt, J.M., Simpson, D.M., Doherty, M.K., Rivers, J., Gaskell, S.J., and Beynon, R.J. (2006) Multiplexed absolute quantification for proteomics using concatenated signature peptides encoded by QconCAT genes. *Nat Protoc* **1**: 1029–1043.

Price, C.W. (2011) The general stress response in *Bacillus subtilis* and related gram-positive bacteria. In *Bacterial Stress Responses*. Storz, G., and Hengge, R. (eds). Washington, DC, USA: ASM Press, pp. 301–318.

Quek, L.-E., Wittmann, C., Nielsen, L.K., and Krömer, J.O. (2009) OpenFLUX: efficient modelling software for ^{13}C-based metabolic flux analysis. *Microb Cell Fact* **8**: 25.

Radmacher, E., and Eggeling, L. (2007) The three tricarboxylate synthase activities of *Corynebacterium glutamicum* and increase of L-lysine synthesis. *Appl Microbiol Biotechnol* **76**: 587–595.

Record, M.T., Jr, Courtenay, E.S., Cayley, D.S., and Guttman, H.J. (1998) Responses of *E. coli* to osmotic stress: large changes in amounts of cytoplasmic solutes and water. *Trends Biochem Sci* **23**: 143–148.

Rohn, H., Hartmann, A., Junker, A., Junker, B.H., and Schreiber, F. (2012) FluxMap: a VANTED add-on for the visual exploration of flux distributions in biological networks. *BMC Syst Biol* **6**: 33.

Rühl, M., Le Coq, D., Aymerich, S., and Sauer, U. (2012)

^{13}C-flux analysis reveals NADPH-balancing transhydrogenation cycles in stationary phase of nitrogen-starving *Bacillus subtilis*. *J Biol Chem* **287**: 27959–27979.

Sauer, U., Hatzimanikatis, V., Hohmann, H.P., Manneberg, M., van Loon, A.P., and Bailey, J.E. (1996) Physiology and metabolic fluxes of wild-type and riboflavin-producing *Bacillus subtilis*. *Appl Environ Microbiol* **62**: 3687–3696.

Schallmey, M., Singh, A., and Ward, O.P. (2004) Developments in the use of *Bacillus* species for industrial production. *Can J Microbiol* **50**: 1–17.

Schilling, O., Frick, O., Herzberg, C., Ehrenreich, A., Heinzle, E., Wittmann, C., and Stülke, J. (2007) Transcriptional and metabolic responses of *Bacillus subtilis* to the availability of organic acids: transcription regulation is important but not sufficient to account for metabolic adaptation. *Appl Environ Microbiol* **73**: 499–507.

Schweder, T., Krüger, E., Xu, B., Jürgen, B., Blomsten, G., Enfors, S.-O., and Hecker, M. (1999) Monitoring of genes that respond to process-related stress in large-scale bioprocesses. *Biotechnol Bioeng* **65**: 151–159.

Singh, K.D., Schmalisch, M.H., Stülke, J., and Görke, B. (2008) Carbon catabolite repression in *Bacillus subtilis*: quantitative analysis of repression exerted by different carbon sources. *J Bacteriol* **190**: 7275–7284.

Sonenshein, A.L., Hoch, J.A., and Losick, R. (2003) *Bacillus subtilis and Its Closest Relatives*. Washington, DC, USA: ASM Press.

Spiegelhalter, F., and Bremer, E. (1998) Osmoregulation of the opuE proline transport gene from *Bacillus subtilis*: contributions of the sigma A- and sigma B-dependent stress-responsive promoters. *Mol Microbiol* **29**: 285–296.

Steil, L., Hoffmann, T., Budde, I., Völker, U., and Bremer, E. (2003) Genome-wide transcriptional profiling analysis of adaptation of *Bacillus subtilis* to high salinity. *J Bacteriol* **185**: 6358–6370.

Street, T.O., Bolen, D.W., and Rose, G.D. (2006) A molecular mechanism for osmolyte-induced protein stability. *Proc Natl Acad Sci U S A* **103**: 13997–14002.

Tännler, S., Decasper, S., and Sauer, U. (2008) Maintenance metabolism and carbon fluxes in *Bacillus* species. *Microb Cell Fact* **7**: 19.

Thiele, T., Steil, L., Gebhard, S., Scharf, C., Hammer, E., Brigulla, M., *et al.* (2007) Profiling of alterations in platelet proteins during storage of platelet concentrates. *Transfusion* **47**: 1221–1233.

Warnes, G., Bolker, B., and Lumley, T. (2013) gplots: various R programming tools for plotting data [WWW document] URL   http://cran.r-project.org/web/packages/gplots/index .html.

Whatmore, A.M., and Reed, R.H. (1990) Determination of turgor pressure in *Bacillus subtilis*: a possible role for K$^+$ in turgor regulation. *J Gen Microbiol* **136**: 2521–2526.

Whatmore, A.M., Chudek, J.A., and Reed, R.H. (1990) The effects of osmotic upshock on the intracellular solute pools of *Bacillus subtilis*. *J Gen Microbiol* **136**: 2527–2535.

van Winden, W.A., Wittmann, C., Heinzle, E., and Heijnen, J.J. (2002) Correcting mass isotopomer distributions for naturally occurring isotopes. *Biotechnol Bioeng* **80**: 477–479.

Winter, T., Winter, J., Polak, M., Kusch, K., Mäder, U., Sietmann, R., *et al.* (2011) Characterization of the global impact of low temperature gas plasma on vegetative micro-organisms. *Proteomics* **11:** 3518–3530.

Wittmann, C. (2002) Metabolic flux analysis using mass spectrometry. In *Tools and Applications of Biochemical Engineering Science*. Schügerl, K., and Zeng, A.-P. (eds). Berlin-Heidelberg, Germany: Springer, pp. 39–64.

Wood, J.M. (2011) Bacterial osmoregulation: a paradigm for the study of cellular homeostasis. *Annu Rev Microbiol* **65:** 215–238.

Yoshida, A. (1965) Enzymic properties of malate dehydrogenase of *Bacillus subtilis*. *J Biol Chem* **240:** 1118–1124.

Young, J.W., Locke, J.C.W., and Elowitz, M.B. (2013) Rate of environmental change determines stress response specificity. *Proc Natl Acad Sci U S A* **110:** 4140–4145.

Zaprasis, A., Brill, J., Thüring, M., Wünsche, G., Heun, M., Barzantny, H., *et al.* (2013) Osmoprotection of *Bacillus subtilis* through import and proteolysis of proline-containing peptides. *Appl Environ Microbiol* **79:** 576–587.

Supporting information

Additional Supporting Information may be found in the online version of this article at the publisher's web-site:

Fig. S1. Workflow used for sample purification, tryptic digestion and LC-MS/MS analysis.

Fig. S2. A. Impact of different NaCl concentrations and; B. Impact of 1 mM of glycine betaine on growth of *Bacillus subtilis* BSB1 (168 Trp[+]) growing on glucose in M9 minimal medium.

Fig. S3. Steady-state extracellular concentrations of acetate and pyruvate during continuous cultivation of *Bacillus subtilis* BSB1 (168 Trp[+]) in M9 minimal medium (1 g l^{−1} glucose, D = 0.1 h^{−1}) under non-stressed (reference) and salt-stressed conditions (stress, 1.2 M NaCl). For osmoprotection, salt-stressed cells were additionally supplemented with 1 mM of glycine betaine.

Fig. S4. Steady-state offgas CO_2 readings during continuous cultivation of *Bacillus subtilis* BSB1 (168 Trp[+]) in M9 minimal medium (1 g l^{−1} glucose, D = 0.1 h^{−1}) under non-stressed (reference) and salt-stressed conditions (stress, 1.2 M NaCl). For osmoprotection, salt-stressed cells were supplemented with 1 mM of glycine betaine.

Fig. S5. Average expression profile of each cluster with standard deviation (left) and enriched functional categories of the Fisher exact test (right). All samples were normalized to the reference condition ($\mu = 0.1$). The functional categories were adopted from the SubtiWiki database (version 2013/2). Number of genes in the enriched functional categories in the cluster X and the total genes in the parent category Y were represented as X of Y.

Table S1. Set of final SRM assay used in this study: Q1 is the mass-to-charge ratio (m/z) for the peptide ion used as Q1 value (precursor ion); Q3 is mass-to-charge ratio (m/z) for the fragment ion used as Q3 value (product ion); CE corresponds to the applied collision energy.

Table S2. Biochemical reaction network and atom transition used for metabolic flux analysis of wild-type *Bacillus subtilis* 168.

Table S3. Theoretical precursor demand [mmol g_{DCW}^{-1}] of wild-type *Bacillus subtilis* 168 during continuous growth at 0.1 h^{−1} on M9 minimal medium without further addition (reference), supplemented with 1.2 M NaCl (salt stress), and supplemented with 1.2 M NaCl and 1 mM glycine betaine (osmoprotection).

Table S4. Comparison between measured and simulated mass isotopomer distribution in proteinogenic amino acids obtained from GC-MS analysis.

Table S5. High-salinity induced genes ($P < 0.05$, at least twofold induced, 0.05 FDR). Assigned gene function was taken from SubtiWiki Version 2013/2 (Mäder *et al.*, 2012).

Table S6. High-salinity repressed genes ($P < 0.05$, at least twofold repressed, 0.05 FDR). Assigned gene function was taken from SubtiWiki Version 2013/2 (Mäder *et al.*, 2012).

Table S7. Induced genes under salt stress in the presence of 1 mM glycine betaine compared with cells under salt stress without osmoprotection ($P < 0.05$, at least twofold induced, 0.05 FDR). Assigned gene function was taken from SubtiWiki Version 2013/2 (Mäder *et al.*, 2012).

Table S8. Repressed genes under salt stress in the presence of 1 mM glycine betaine compared with cells under salt stress without osmoprotection ($P < 0.05$, at least twofold repressed, 0.05 FDR). Assigned gene function was taken from SubtiWiki Version 2013/2 (Mäder *et al.*, 2012).

Appendix S1. Transcriptome analysis protocol.

Appendix S2. Quantitative proteome analysis protocol.

Appendix S3. Metablome analysis protocol.

Appendix S4. Global transcriptional response of *Bacillus subtilis* to salt stress and osmoprotection.